Science of Remote Sensing 9 (2024) 100120

Contents lists available at ScienceDirect

Science of Remote Sensing

journal homepage: www.sciencedirect.com/journal/science-of-remote-sensing

Remotely characterizing photosynthetic biocrust in snowpack-fed microhabitats of Taylor Valley, Antarctica

Sarah N. Power [a,*], Mark R. Salvatore [b], Eric R. Sokol [c], Lee F. Stanish [d], Schuyler R. Borges [b], Byron J. Adams [e,f], J.E. Barrett [a]

[a] Department of Biological Sciences, Virginia Polytechnic Institute and State University, 2125 Derring Hall, Mail Code 0406, 926 West Campus Drive, Blacksburg, VA, 24061, USA
[b] Department of Astronomy & Planetary Science, Northern Arizona University, NAU Box 6010, Flagstaff, AZ, 86011, USA
[c] National Ecological Observatory Network, Battelle Memorial Institute, 1685 38th Street, Suite 100, Boulder, CO, 80301, USA
[d] Institute of Arctic and Alpine Research, University of Colorado, Campus Box 450, Boulder, CO, 80309, USA
[e] Department of Biology, Brigham Young University, 4127 LSB, Provo, UT, 84602, USA
[f] Monte L. Bean Life Science Museum, 645 E 1430 N, Provo, UT, 84602, USA

ARTICLE INFO

Keywords:
Antarctica
Biocrust
Carbon
Reflectance spectroscopy
Snow
Soil ecology

ABSTRACT

Microbial communities are the primary drivers of carbon cycling in the McMurdo Dry Valleys of Antarctica. Dense microbial mats, consisting mainly of photosynthetic cyanobacteria, occupy aquatic areas associated with streams and lakes. Other microbial communities also occur at lower densities as patchy surface biological soil crusts (hereafter, biocrusts) across the terrestrial landscape. Multispectral satellite data have been used to model microbial mat abundance in high-density areas like stream and lake margins, but no previous studies have investigated the lower detection limits of biocrusts. Here, we describe remote sensing and field-based survey and sampling approaches to study the detectability and distribution of biocrusts in the McMurdo Dry Valleys. Using a combination of multi- and hyperspectral tools and spectral linear unmixing, we modeled the abundances of biocrust in eastern Taylor Valley. Our spectral approaches can detect low masses of biocrust material in laboratory microcosms down to biocrust concentrations of 1% by mass. These techniques also distinguish the spectra of biocrust from both surface rock and mineral signatures from orbit. We found that biocrusts are present throughout the soils of eastern Taylor Valley and are associated with diverse underlying soil communities. The densest biocrust communities identified in this study had total organic carbon 5x greater than the content of typical arid soils. The most productive biocrusts were located downslope of melting snowpacks in unique soil ecosystems that are distinct from the surrounding arid landscape. There are similarities between the snowpack and stream sediment communities (high diversity of soil invertebrates) as well as their ecosystem properties (*e.g.*, persistence of liquid water, high transfer of available nutrients, lower salinity from flushing) compared to the typical arid terrestrial ecosystem of the dry valleys. Our approach extends the capability of orbital remote sensing of photosynthetic communities out of the aquatic margins and into the drier soils which comprise most of this landscape. This interdisciplinary work is critical for measuring and monitoring terrestrial carbon stocks and predicting future ecosystem dynamics in this currently water-limited but increasingly dynamic Antarctic landscape, which is particularly climate-sensitive and difficult to access.

1. Introduction

Biocrusts, *i.e.*, soil aggregates containing communities of cyanobacteria, algae, moss, lichen, *etc*. on the surface of soil (Weber et al., 2022), inhabit all continents (Belnap et al., 2016), are estimated to cover 12% of the Earth's terrestrial surface (Rodriguez-Caballero et al., 2018), and play foundational roles in the ecosystems where they occur (Belnap et al., 2016). Biocrusts are distributed across hot and cold deserts and are oftentimes an important source, if not the primary source, of carbon (C) in these systems (Elbert et al., 2012). They perform key ecological functions, including photosynthesis, nitrogen fixation, nutrient cycling, and soil stabilization (Belnap, 2003), which are particularly important

* Corresponding author.
E-mail address: snpower@vt.edu (S.N. Power).

https://doi.org/10.1016/j.srs.2024.100120
Received 13 June 2023; Received in revised form 1 February 2024; Accepted 5 February 2024
Available online 6 February 2024

in ecosystems that lack vascular vegetation. Biocrusts may be more susceptible to climate change than previously thought (Finger-Higgens et al., 2022). Climate warming and precipitation variation appears to have already impacted some biocrust communities and will likely continue to result in biocrust degradation across ecosystems (Finger--Higgens et al., 2022). Detecting and mapping biocrust is essential for monitoring these important soil communities in a changing climate.

In the McMurdo Dry Valleys (MDV) of Antarctica, microbial communities are the drivers of carbon cycling, particularly in and adjacent to lakes, ponds, and streams where dense microbial mats are abundant (Cary et al., 2010; Van Horn et al., 2016; Stone et al., *accepted*). However, less dense microbial communities also occur in drier soils outside the hydrological influence of glaciers, stream channels, or lakes in areas where snow or subsurface thaw are presumably the main sources of water. In such environments, which constitute most of the dry valley landscape, microbial communities are sparse, have high soil content, and are better described as biocrusts. Here, we define biocrusts as the communities which are present in drier areas away from streams and lakes, and although they can be quite similar morphologically to the microbial mats present in aquatic areas, biocrusts are typically less dense and patchily distributed among the terrestrial landscape where there are alternative sources of moisture, *e.g.*, snowpacks and groundwater seeps (Gooseff et al., 2013; Weber et al., 2022).

Previous studies of MDV microbial mat dynamics have primarily focused on the communities occurring close to or within the streams and lakes (*e.g.*, Alger et al., 1997). Soil environments outside of stream channels have traditionally been thought to support less visible biocrust biomass in comparison, so fewer studies have focused on these terrestrial communities. However, these terrestrial areas are far more spatially extensive than the aquatic environments in the MDV, and therefore, even sparse distributions and densities of biocrusts could sum to a considerable amount of total biomass. For example, the Lake Fryxell basin, excluding Lake Fryxell, is 53.55 km^2, while the cumulative stream area is approximately 2.58 km^2 (4.82%), determined via satellite imagery. The terrestrial landscape of this region occupies more than 20*x* the surface area relative to ephemeral stream channels and lake margins, so although biocrusts are typically less dense than microbial mats, we anticipate soils of the MDV contain a considerable amount of carbon in and under these biocrusts (*e.g.*, Burkins et al., 2001). We suggest that the terrestrial regions of Taylor Valley may contain more cumulative biomass than the stream channels given their spatial extent. A systematic and scalable method is required to measure and monitor biocrust biomass over large spatial scales: remote sensing.

Assessing the detectability of biocrusts via remote sensing is a critical first step in estimating terrestrial carbon stocks in this region and examining controls over the distribution and activity of these soil communities. Our previous research has demonstrated the utility of multispectral satellites (*e.g.*, WorldView-2 and WorldView-3; WV-2 and WV-3) in detecting densely colonized microbial mats near streams in the Lake Fryxell basin region using spectral parameters and spectral linear unmixing models (Power et al., 2020; Salvatore, 2015; Salvatore et al., 2020, 2021). In addition to the strong photosynthetic signatures identified near stream channels and lake margins, we also observed enhanced spectral signatures indicative of photosynthetic activity in upland areas not connected to streams or lakes (Power et al., 2020). While remote sensing techniques have been demonstrated to be effective in regions of dense microbial mats, these techniques have not been specifically validated throughout the broader landscape where photosynthetic communities are much more dispersed and their resultant signatures are often much weaker and discontinuous. Therefore, this work tests the hypothesis that these observed spectral signatures outside of stream channels are associated with areas of increased soil productivity and not, for example, associated with spectral artifacts created by topographic or lithological variations.

Our objectives for this study are to assess the detectability of biocrust and examine the environments in which these unique communities are found in the MDV. By investigating the spatial distribution of biocrusts using orbital data, our work contributes in part to efforts in refining existing carbon budgets (*e.g.*, Barrett et al., 2006b; Burkins et al., 2001), predicting future carbon stocks, and examining controls over the distribution and activity of biocrusts in the MDV. Here, we present the first assessment of biocrust detectability in the MDV terrestrial landscape using a combination of laboratory hyperspectral spectroscopy, WorldView-2 and WorldView-3 multispectral satellite imagery, and *in-situ* soil and biocrust surveying and sampling.

2. Materials and methods

2.1. Site description

The MDV are the largest contiguous ice-free area on the Antarctic continent, with approximately 4500 km^2 of exposed soil, stream, and lake ecosystems (Levy, 2013). Glacial meltwater during the austral summer (*i.e.*, 24 h daylight) feeds streams that flow for an average of 4–9 weeks per year (Wlostowski et al., 2016). These streams drain into perennially ice-covered lakes along the floor of Taylor Valley. While dense microbial mats (mm – cm thick) occupy streams and lake margins (Fig. 1 a), biocrusts occur at lower densities as discontinuous mats in intermittently wet soils (Fig. 1 b, c). The microbial mats are dominated by cyanobacteria (*e.g.*, *Nostoc*, *Oscillatoria*, and *Phormidium*) and also contain chlorophyta (green algae) (Alger et al., 1997), various diatom species (Alger et al., 1997), and mosses which can also occur separately from microbial mats (*Bryum* spp. and *Hennediella* spp.; Pannewitz et al., 2003; Schwarz et al., 1992). While studies on biocrust composition in the MDV are lacking, the biocrusts here contain cyanobacteria and mosses based on visual identification and appear to be dominated by *Nostoc* specifically. Communities of nematodes, rotifers, and tardigrades also inhabit the soils, sediments, and microbial mats of this region (Freckman and Virginia, 1997; Simmons et al., 2009a). Though, given the relatively low soil invertebrate biomass, grazing influences on microbial mats and biocrusts are thought to be minimal, making the MDV a simple system for studying biocrust and microbial mat dynamics.

Taylor Valley, one of several valleys in the MDV, spans from the McMurdo Sound of the Ross Sea in the east to the Taylor Glacier in the west. The eastern portion of Taylor Valley includes a dozen ephemeral glacial meltwater streams and Lake Fryxell, which have been the subject of numerous microbial mat studies (*e.g.*, Alger et al., 1997; Kohler et al., 2015; McKnight et al., 1998; Stanish et al., 2011). Due to proximity to the coast, eastern Taylor Valley also has the greatest relative humidity and the most shallow ice-cemented permafrost layers in the region, and therefore typically has higher soil water content (Bockheim et al., 2008; Doran et al., 2002; Obryk et al., 2020) and richer communities of soil invertebrates with greater biomass than other parts of Taylor Valley or neighboring Wright Valley (Adams et al., 2006; Barrett et al., 2006c, 2007; Courtright et al., 2001; Xue et al., 2023).

2.2. Spectral detection limit experiment

We created microcosms of biocrust material and bare soil (not containing biocrust) of varying percent (0–100%) biocrust by weight (g/g) in the laboratory and characterized these materials using hyperspectral reflectance techniques to quantify the potential detection limits of our remote sensing methods. The soil was collected from the Fryxell basin, and to minimize oversampling of the sensitive dry valley biocrust communities, we collected a *Nostoc*-dominated biocrust from a warm desert environment in Arizona, which has a similar spectrum as the dry valley biocrust (Fig. S1). Both biocrust spectra contain absorption features at ~0.68, 1.19, 1.45, 1.78, and 1.93 μm, indicating that the major spectral characteristics between both types of biocrust are the same and therefore justify this analog material's appropriateness for our laboratory experiment. The biocrust and soil were separately ground into a homogenous fine particle size for hyperspectral analysis. This

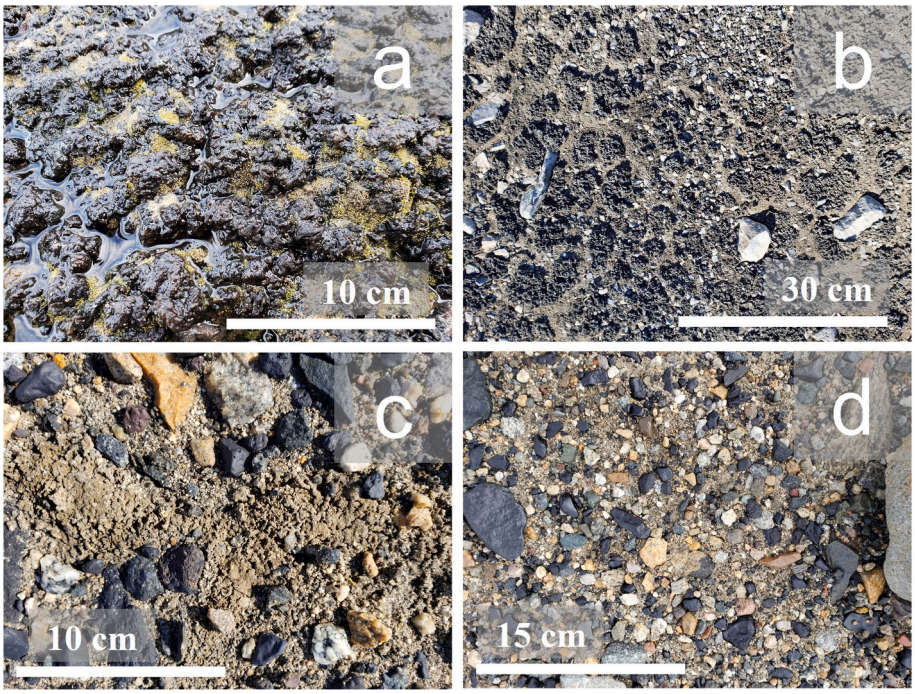

Fig. 1. Photos of (**a**) dense, wet microbial mat in the Canada Flush (see Power et al., 2020); (**b**) dense biocrust downhill from snowpack (plot 09); (**c**) sparse, incipient biocrust in moist depression (plot 26); and (**d**) representative low productivity desert pavement (plot 31). Photographs taken by S. Power.

disaggregation process allows the biocrust to evenly distribute among the soil particles, and from a chemical and pigment perspective, the spectral characteristics of the biocrust remain largely unchanged after disaggregating. A known quantity of biocrust was mixed with a known quantity of soil to achieve the desired percent biocrust mixtures, and the mixtures were placed into a sample holder ~2.5 cm in diameter and 0.5 cm in depth. Sample mixtures were moistened with DI water and placed under a halogen lamp for several minutes, allowing time for the organisms to reactivate and begin photosynthesizing. We targeted a final water content for our wetted samples of approximately 0.25 GWC (g H_2O/g dry soil and biocrust material). Spectra were acquired using an Analytical Spectral Devices (ASD) FieldSpec4 high-resolution hyperspectral reflectance spectrometer set up for use in a stable lab environment. Data were collected between 350 and 2500 nm at a 1 nm sampling interval. A halogen lamp was used to illuminate the samples at 30° off-nadir and approximately 25 cm away, while reflectance was measured at nadir using the ASD's bare fiber optic cable roughly 3 cm above the sample surface with a 25° field of view projecting a 1.39 cm^2 spot size onto our samples. To minimize instrument noise, particularly at the longest and shortest wavelengths where the output of the halogen bulb is lowest, we averaged 50 individual spectra for each biocrust-soil combination produced in the lab. All data were then downsampled to WV-2 and WV-3 spectral resolutions for direct comparison to the respective orbital platforms. Linear mixtures of pure soil and biocrust spectra were also modeled for comparison to the spectra of those known physical mixtures to determine the nature of the observed spectral mixing relationship, validating the ability to confidently translate this linear unmixing method to orbital data.

2.3. Orbital spectral collection and processing

Satellite images acquired during austral summers were used to identify photosynthetic signatures in upland terrestrial areas. WorldView-2 and WorldView-3 (DigitalGlobe, Inc.) are multispectral satellites in polar orbit with 8 multispectral bands at 1.84 m and 1.24 m nadir resolutions, respectively. Georeferenced data, validated using ground control points, were obtained from the University of Minnesota Polar Geospatial Center (PGC) through a cooperative agreement between the National Science Foundation (NSF) and National Geospatial-Intelligence Agency (NGA). These data were subsequently processed to atmospherically corrected surface reflectance using five spectral ground validation targets acquired in the field during the 2018–2019 austral summer, following methods from Salvatore et al. (2021). Band-specific linear relationships between top-of-atmosphere reflectance data and ground validation spectra were applied to the entirety of the satellite images to remove atmospheric contributions to the observed signal. These corrected surface reflectance data were used in several analyses and compared with ground-based surveys of soil chemical and biological properties detailed in the sections below.

2.4. Field site identification and in-situ environmental sample collection

We used vegetation indices, such as the Normalized Difference Vegetation Index parameter (NDVI; Tucker, 1979), to target locations of varying photosynthetic activity across the eastern Taylor Valley landscape. High NDVI values are typical of photosynthetic vegetation, which has a unique spectral signature of absorbance in the visible wavelengths (due to the activity of chlorophyll-a and other pigments) and strong reflectance in near-infrared regions due to scattering and reflectance of long-wave radiation by cell walls. NDVI was calculated using spectral reflectance measurements acquired in the near-infrared (WV-2 Band 7, centered at 831 nm; WV-3 centered at 832 nm) and red (WV-2 Band 5, centered at 659 nm; WV-3 centered at 661 nm) using the Environment for Visualizing Images (ENVI, Harris Geospatial) software package.

Thirty locations with either consistently high NDVI values, consistently low NDVI values, or variable NDVI values were identified in eastern Taylor Valley outside of stream channels and lake margins (Fig. 2) using three satellite images: a WV-3 image acquired on January 17, 2015 (1040010006846000), a WV-2 image acquired on January 19, 2018 (1030010077755100), and another WV-2 image acquired on December 11, 2018 (1030010089D13500). These 30 locations were selected to represent a range of potential photosynthetic activity and topographic features (*i.e.*, slope, aspect, and elevation) characterized using an airborne lidar-derived digital elevation model (DEM) at 1 m

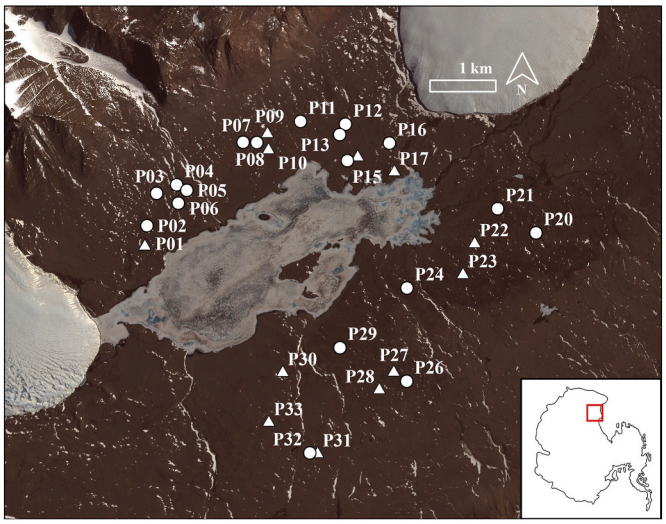

Fig. 2. True color image of the Lake Fryxell basin with the 30 sampling locations labeled. The 12 intensively sampled plots are denoted by triangles. Inset on the bottom right corner identifies the McMurdo Dry Valleys, Antarctica with a red square. WV-2 imagery (1030010089D13500) © Dec 11, 2018 DigitalGlobe, Inc. (For interpretation of the references to color in this figure legend, the reader is referred to the Web version of this article.)

spatial resolution (Fountain et al., 2017). Depressions, rocky outcrops, sloped hills, and flat surfaces were all represented in our field locations. Overall, these locations were selected to maximize spatial coverage of ranges in photosynthetic activity and topography across the landscape.

We sampled, photographed, and documented relevant environmental conditions (*e.g.*, evidence of surface moisture, presence/absence of microbial mat, moss, or biocrust, presence of snowpacks, surface or lithological variations like dominant presence of oxidized granite) at each of these 30 locations in December of 2019. We collected a surface layer sample of soil or biocrust (if present) and rock from all sites for subsequent hyperspectral analysis in the laboratory using the same methods and laboratory set-up as previously described in Section 2.2. At 12 of the sites, we established 5 m × 5 m intensive sampling plots and collected 5 surface layer soil or biocrust samples 128 cm^2 in area from each corner and center of the plots for pigment analysis (chlorophyll-a, scytonemin, and carotenoids) and organic matter content via ash-free dry mass (AFDM). We also collected underlying soil down to 10 cm below the surface for gravimetric water content (GWC), electrical conductivity (EC), pH, inorganic nitrogen (N) concentration in the form of ammonium (NH_4^+) and nitrate (NO_3^-), inorganic phosphorus (P) concentration in the form of phosphate (PO_4^{3-}), total organic carbon (TOC), total nitrogen (TN), and invertebrate abundance (see below). After the initial soil chemistry and invertebrate diversity and abundance analyses, samples were frozen at −20 °C and transported to Virginia Tech and Northern Arizona University for remaining chemical and spectral analyses.

2.5. Analysis of environmental field samples

We estimated pigment concentration on the surface ~1 cm layer soil and biocrust samples using a trichromatic spectrophotometric method for chlorophyll-a, carotenoids, and scytonemin at 663, 490, and 384 nm, respectively (Garcia-Pichel and Castenholz, 1991). Throughout the process, care was taken to avoid exposing the samples to light. The samples were dried at 105 °C for 24 h, sieved through a 4 mm sieve, and extracted for 24 h at ambient temperature in 90% unbuffered acetone using a 3.75:10 soil to solvent ratio, based on protocols from Couradeau et al. (2016) and the McMurdo Dry Valleys Long Term Ecological Research Program (MCM LTER) standard methods. After centrifugation, the extracts were analyzed on a spectrophotometer using 10 mL cuvettes. The absorbances contributed by each pigment were calculated using the trichromatic equations outlined in Garcia-Pichel and Castenholz (1991), and the pigment concentrations were calculated using the Beer-Lambert Law with the extinction coefficients of 89.7 L g^{-1} cm^{-1} for chlorophyll-a (Couradeau et al., 2016), 112.6 L g^{-1} cm^{-1} for scytonemin (Brenowitz and Castenholz, 1997), and 262 L g^{-1} cm^{-1} for carotenoids (Thrane et al., 2015). Additionally, the surface layer soil and biocrust samples were measured for AFDM by weighing a known area of sample, combusting at 550 °C for 24 h using a muffle furnace, gently stirring samples halfway through combustion, and reweighing after cooling in a desiccator. Given the very low clay content of soils in this region (Barrett et al., 2006a), the rehydration of clays was assumed negligible, so we did not rewet samples.

Using the underlying 1–10 cm soil, we measured pH and electrical conductivity using a 1:2 and 1:5 soil to DI H_2O slurry with pH and conductivity probes, respectively (Barrett et al., 2004), and we measured gravimetric water content by mass lost after oven drying at 105 °C for 24 h. We also extracted inorganic N (NH_4^+ and NO_3^-) in 2 M potassium chloride and inorganic P (PO_4^{3-}) in 0.5 M sodium bicarbonate; inorganic N and P were measured on extracts using a Lachat QuikChem flow injection analyzer (Keeney and Nelson, 1982; Olsen and Sommers, 1982; Knepel, 2003; Prokopy, 1995). Additionally, we measured TOC and TN using an Elementar Vario MAX Cube analyzer after fumigating samples with concentrated hydrochloric acid to remove the influence of carbonates on TOC values (Ramnarine et al., 2011; Walthert et al., 2010; Fritsen et al., 2000).

Invertebrate abundance was enumerated using inverted light microscopy on soil solutions using a modified sugar-centrifugation extraction procedure described by Freckman and Virginia (1993). Nematode abundance is reported as the total number of live *Scottnema*, *Eudorylaimus,* and *Plectus* individuals, and total live rotifers and tardigrades per kg dry mass soil. Using R Statistical Software version 4.0.3 (R Core Team, 2017), a PCA on correlation was executed to visually compare plots in terms of their physicochemical properties. A MANOVA was performed to statistically assess whether there is a significant difference between the three plot types (biocrust, oxidized granite, soil) using physicochemical variables. An ANOVA was performed next to assess which, if any, physicochemical variables are significantly different between the plot types.

2.6. Vegetation index analysis using orbital data

To examine variations in photosynthetic activity across our sampled locations in eastern Taylor Valley, we applied several vegetation indices to orbital data. The primary WV-2 image used in this analysis (103001009FA0AE00) was acquired on December 3, 2019, approximately three weeks before our field sampling campaign. In addition to NDVI, we also calculated the Simple Ratio Index (SR), the Red-Edge Simple Ratio Index (SRre), and the Normalized Pigment Chlorophyll Index (NPCI). SR and NPCI are effective in detecting dry biocrust communities from other arid regions (*e.g.*, the Colorado Plateau) with a portable spectroradiometer (Young and Reed, 2017). SR was calculated using the NIR and red bands, SRre was calculated using the NIR and red-edge bands, and NPCI was calculated using the red and coastal bands. Each of the parameter values were extracted from the four pixels centered at each of the plot locations, based on handheld GPS coordinates taken during sampling and visually confirming plot location via nearby boulders, snowpacks, *etc*. These values were averaged to estimate an average NDVI, SR, SRre, and NPCI value for each of the plots. Average reflectance values for each of the eight WV-2 bands were calculated for each plot as well. Using R Statistical Software version 4.0.3 (R Core Team, 2017), a correlation matrix was constructed with the vegetation indices and raw bands to investigate any significant relationships between these primary remote sensing data and biological parameters collected *in-situ* (AFDM and pigment concentration). A

principal components analysis (PCA) on covariance was executed to visually compare plots in terms of their orbital reflectance spectra (raw bands B1 – B8). A multivariate analysis of variance (MANOVA) was performed to statistically assess whether there is a significant difference between the three plot types (biocrust, oxidized granite, soil) using the multispectral bands. A univariate analysis of variance (ANOVA) was performed next to assess which, if any, spectral bands and vegetation indices (NDVI, SR, SRre, NPCI) are significantly different between the plot types. Plot 11 and plot 21 were excluded from these three statistical analyses because they were covered in snow and therefore their reflectance data skewed the analyses.

2.7. Spectral linear unmixing of orbital data

Spectral linear unmixing was used to model the spectral contribution of individual surface types, and therefore calculate the fractional abundance of each surface type per pixel (Lawson and Hanson, 1974; Adams et al., 1993; Ramsey and Christensen, 1998; Bioucas-Dias et al., 2012; Salvatore et al., 2020). Spectral unmixing uses a library of 'pure' spectral endmembers of each surface type to train the model by matching the measured spectral signature, while reducing the misfit between the measured and modeled spectra. Endmembers are limited to the number of spectral bands and degrees of freedom in the data that are being unmixed; therefore, we were constrained to eight or fewer endmembers for unmixing using the WV-2 and WV-3 satellites (Adams et al., 1993; Ramsey and Christensen, 1998). Our seven hyperspectral endmembers were derived through collection in the field, collection after laboratory preparation, or were modeled from field experiments. Six of these endmembers (black microbial mat, orange microbial mat #1 and #2, water, moss, and soil) were previously used in this region and are described in detail in Salvatore et al. (2021), and one additional endmember (an orange oxidized granite) was added for an updated emphasis on the terrestrial landscape and was collected during our field campaign and subsequently measured in the laboratory. This granite endmember is from a minor subunit of the broader Granite Harbour Intrusive Complex that outcrops near the top walls of Taylor Valley (Cox et al., 2012). X-ray diffraction confirmed the dominance of quartz (~30%), plagioclase feldspar (~25%), alkali feldspar (~25%), and mafic and other ancillary phases (~20%), while VNIR reflectance spectroscopy indicated a crystalline Fe-oxide phase, likely goethite or hematite, at orbitally relevant wavelengths. As a result of these analyses, we refer to this endmember as "oxidized granite." All seven spectra were downsampled to WV-2 and WV-3 resolutions to create a spectral library that was used to unmix the entirety of each orbital image. Snow and ice were not included as spectral endmembers despite their pervasiveness across the landscape, because both snow and ice are known to exhibit significant VNIR spectral variability. For example, variations in snow crystallinity, grain size, liquid water content, and impurity content all have significant spectral influences (Warren, 1982). Instead, snow was identified in unmixed images using a combination of both high root-mean-square errors (RMSE) and high VNIR albedo.

Linear unmixing is less commonly used in the visible or near-infrared portions of the electromagnetic spectrum in more vertical ecosystems where multiple scattering can be significant, (*i.e.* between vegetation canopy layers). Here, however, we assume minimal spectral contributions from volumetric scattering with depth in the largely barren surface environments of the MDV where linear unmixing has been demonstrated successfully (Salvatore et al., 2020, 2021). Because of these assumptions and their demonstrated effectiveness in the past, we have selected linear unmixing as an appropriate method for this study (Peddle et al., 1999; Roberts et al., 1993; Salvatore et al., 2020, 2021).

An 'early season' December 21, 2021 WV-2 image (10300100CB9F3900) and a 'late season' January 21, 2015 WV-2 image (103001003ED2B400) were the primary images used in this unmixing analysis to capture potential seasonal variation in the spectral signatures of biocrusts and soils. The DaVinci software package was used to run the unmixing model, using our seven spectral endmembers to linearly derive the areal abundance of these different surface components. The results include percent surface abundance as well as RMSE, which provides a measure of the goodness of fit between the input spectrum and the modeled spectrum. Abundance estimates from each of the endmembers were extracted from the 30 plot locations, incorporating a buffer to confidently capture the plot area (25 pixels per plot). RMSE were analyzed for each pixel-level abundance estimate, commonly ranging between ~0.1% to below 0.4%. However, certain pixels contained high RMSE and were attributed to being covered in snow, as verified by examining albedo estimates and the true-color WV-2 images. To account for the uncertainty imposed by snow in these areas, we filtered the abundance data by applying a threshold of RMSE >0.5%. Any pixels that contained RMSE >0.5% were removed from the analysis.

To qualitatively and quantitatively assess the unmixing model output for an early season and late season image, we selected 15 plots to examine abundances of the different surface types. These plots were visually categorized in the field as having either biocrust/incipient biocrust, soil, or oxidized granite (*i.e.*, 5 biocrust/incipient biocrust, 5 soil, and 5 oxidized granite plots). The orange microbial mat #1 and #2 endmember abundances were aggregated into a single orange mat group abundance, and we combined the soil endmember and water endmember abundances together as 'other abiotic' abundance. We compared our field measurements to our modeled total biocrust abundance, which was calculated as the sum of modeled black microbial mat, orange microbial mat, and moss abundance estimates for each pixel. While it is unlikely for all three of these microbial mat communities to co-occur in the environments we assessed outside of stream channels (Alger et al., 1997), summing all biological endmembers to create a "total biocrust abundance" parameter provides a quantitative assessment of the spectral contributions of photosynthetic pigments and the reflective structure of living cells. Therefore, this parameter is effective for the purposes of distinguishing surfaces where photosynthetic signatures are present, and our efforts will help to quantify our abilities to derive the abundances of these communities remotely.

2.8. Albedo analysis of orbital data

We selected 13 cloud-free WorldView images acquired between 2009 and 2019 (six images acquired in December and seven images acquired in January) (Table S1) to determine how the landscape's albedo changes from the 'early season' to the 'late season' and to therefore examine the potential presence of ephemeral snowpacks in the vicinity of our study plots, which based upon our field surveys were often associated with visible biocrust communities. Moreover, the presence of snowpack can mask surface soil features, so it was necessary for our analyses to characterize snowpacks in the vicinity of our plots. The mean and standard deviation of each pixel in these suites of early and late season images can provide important information related to surface landscape features. For example, brightening of surfaces indicates the presence of salts or snow on the surface, while darkening typically indicates increased soil moisture. We assume that topographic variations resulting in variations in shadows are negligible on the valley floor for the purposes of this exercise. We predict that surfaces dominated by abiotic materials (granite and soil) will experience less variability in albedo over time than areas exhibiting increased photosynthetic and/or hydrological activity. After stacking the December and the January images, the average albedo and albedo standard deviation (SD) were calculated for each of the 25 pixels surrounding each plot's center. Plot-level average and SD albedo were then calculated for December and January, separately. These data were plotted against one another and visualized based on identified surface type (biocrust, granite, soil) to analyze any associations with albedo and seasonality.

3. Results

3.1. Laboratory spectral validation study

Hyperspectral measurements of the soil biocrust microcosms exhibited significant chlorophyll absorption features at ~0.68 μm for all mixtures containing biocrust (Fig. 3), including the lowest abundance sample of 1% biocrust by weight (g/g). Lab measurements of the two extreme spectra (100% soil and 100% biocrust) were downsampled to WorldView resolution to compare with the resolution of the orbital data available for the field plots and were used to unmix spectra of actual biocrust mixtures measured in the lab. There was a strong linear fit between the modeled and measured biocrust abundance with an R^2 of 0.99 and p-value <0.001 (Fig. 4). Mixtures of biocrust and soil combine linearly in VNIR spectral space in these ideal conditions, demonstrating how linear unmixing models can successfully predict biocrust abundance.

3.2. Field surveys and spectral analyses

We found that many of the high or variable NDVI locations occurred in areas near snowpacks and in the lee of hills or in depressions (*i.e.*, nivation hollows; Eveland et al., 2013), where biocrust cover over desert pavement was visually evident. One location in particular had visibly wet soils and dense biocrusts, plot 09 (Fig. 5 a, d, g). Percent coverage of up to 47% biocrust and average surface AFDM of 280 g m^{-2} of biocrust in plot 09 is similar to the lower range of densities reported for microbial mats on riparian sediments adjacent to nearby stream channels (Alger et al., 1997; Power et al., 2020; Salvatore et al., 2021). In contrast, several plots were extremely dry with no visible biocrust but had oxidized granite boulders and relatively high NDVI from orbital data (Fig. 5 b, e, h). Hyperspectral VNIR measurements collected from the field plot samples exhibited clear spectral differences between plots with visible presence of biocrust, granite boulders, and typical desert pavement soil (Fig. 5 j, k, l). Additionally, some plots were visually characterized as having sparse, incipient biocrust with weak but significant chlorophyll absorptions (*e.g.*, P04, P11; Fig. 6). We ranked each plot on biocrust presence as "not present", "possibly present", "likely present", and "present" based entirely on visual observations in the field, finding that plots where biocrust was present or was likely present had overall higher NDVI values using the hyperspectral VNIR measurements (Fig. 7). Plots that were dominated by oxidized granite also had relatively high NDVI but lacked visible biocrust. The densest biocrust plot and the granite boulder plots had relatively high NDVI based on the hyperspectral data as well; however, the shapes of their spectral signatures are very different (*e.g.*, biocrust plot 09 and oxidized granite plot 20; Fig. 5 j, k; Fig. S2).

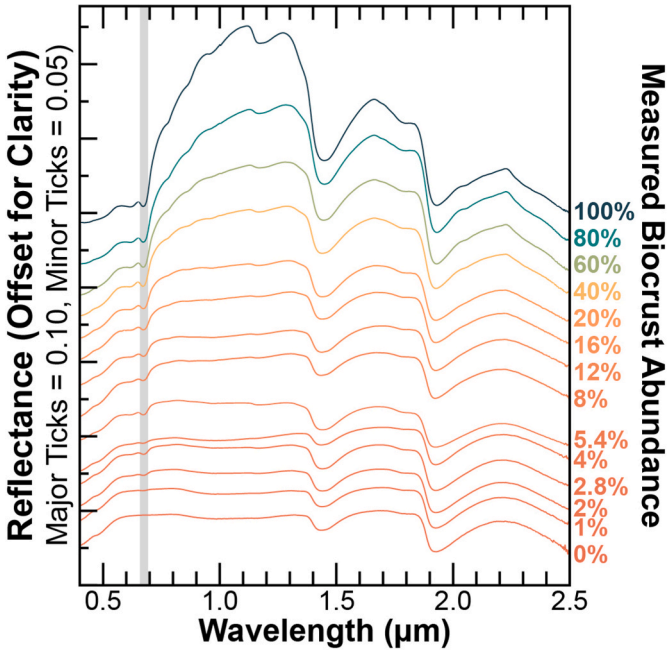

Fig. 3. Hyperspectral signatures of wetted laboratory mixtures of soil and biocrust at varying abundances. Reflectance offset to distinguish each spectra separately. Listed percentages indicate measured biocrust by weight. Chlorophyll absorption feature identifiable at ~0.68 μm, denoted by vertical gray bar.

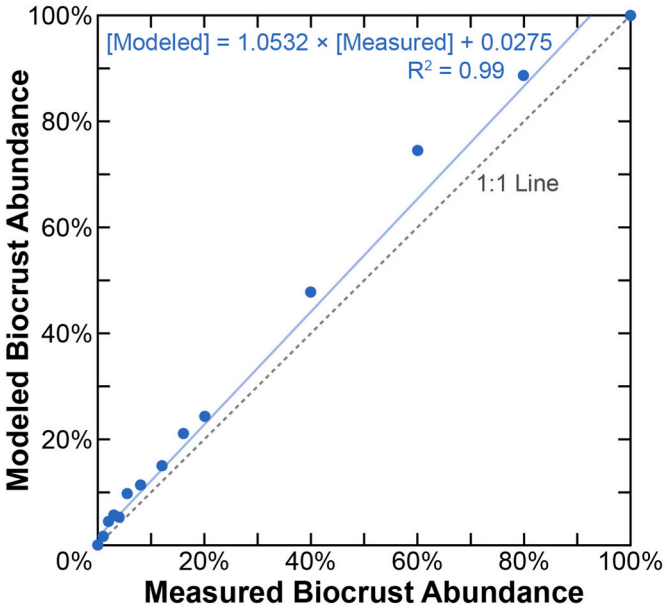

Fig. 4. Scatterplot showing modeled vs. measured biocrust abundance determined in laboratory experiment. Highly significant fit (R^2 = 0.99, p-value <0.001) between modeled (spectral linear unmixing) and measured biocrust abundance using laboratory mixtures of soil and biocrust.

In a PCA on covariance using the WV-2 band reflectance (B1 – B8), plot types are significantly differentiated using multispectral band data (MANOVA, p-value = 0.048) (Fig. 8). Notably, the plots with oxidized granite are spectrally dissimilar from the biocrust and soil plots when all eight bands are used. It is also possible to distinguish among plot types using common vegetation indices (ANOVA; NDVI p-value <0.001; SR p-value <0.001; SRre p-value <0.01; NPCI p-value <0.01). Particularly, oxidized granite plots have significantly higher values for all vegetation indices compared to the biocrust and soil plots. In a correlation matrix between the vegetation indices, raw reflectance bands, and biological parameters (AFDM, chlorophyll, and scytonemin concentration), there are no significant relationships between these primary remote sensing data and biological parameters (Table S2).

3.3. Soil characterization

There was significant variation in pigments, organic matter, invertebrate populations, (Table 1) and in other physical and chemical variables (Table 2) among the plots. Notably, plot 09, with dense biocrust, had the highest abundances and diversity of soil invertebrates, hosting three nematode taxa (*Scottnema*, *Eudorylaimus*, and *Plectus*) in addition to tardigrades, rotifers, and ciliates, similar to the community composition found in soils near streams (Ayres et al., 2007; Simmons et al., 2009a; Treonis et al., 1999). While *Scottnema* was present in relatively high abundances throughout most plots (as has been previously reported for this area of Taylor Valley; Courtright et al., 2001), there were several plots (P22, 30, 31) without any invertebrates present where distinct soil chemistry (pH, nitrate, and electrical conductivity) likely created

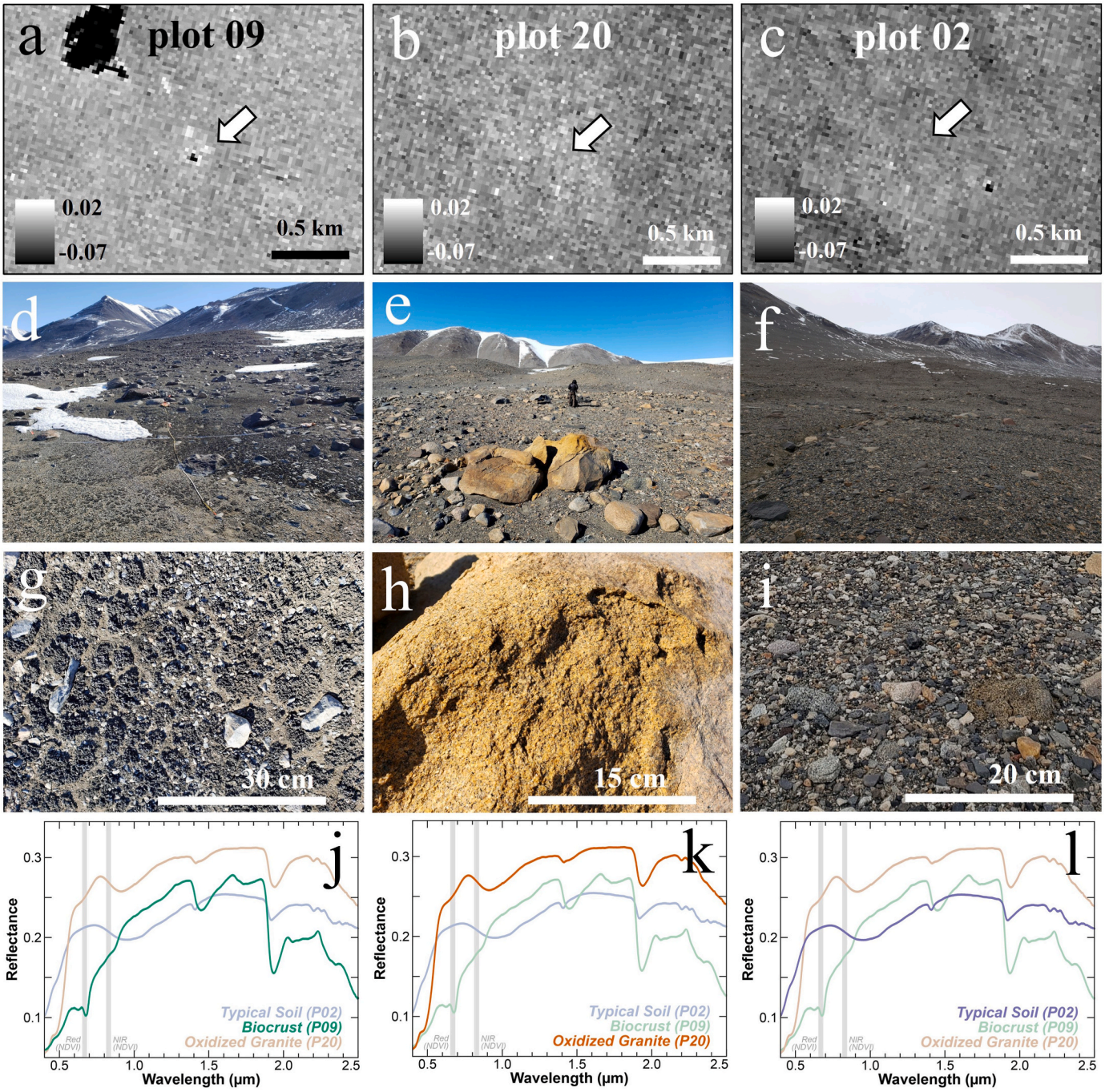

Fig. 5. Orbital NDVI images of (**a**) relatively high NDVI area of plot 09, (**b**) relatively high NDVI area of plot 20, and (**c**) relatively low NDVI area of plot 02. Landscape photos of (**d**) dense biocrust downhill from snowpack (plot 09), (**e**) oxidized, weathered granite boulder field (plot 20), and (**f**) typical low productivity desert pavement (plot 02). Close up photos of the (**g**) dense biocrust, (**h**) oxidized, weathered granite, and (**i**) typical desert pavement. Hyperspectral reflectance signature of (**j**) plot 09 biocrust, (**k**) plot 20 oxidized granite, and (**l**) plot 02 typical soil with each separate spectra transparent in background. Gray bars outline the region of NDVI calculation (steeper slope illustrates higher NDVI). Photographs taken by S. Power. WV-3 imagery (10400100485D6900) © Jan 26, 2019 DigitalGlobe, Inc.

inhospitable conditions (*e.g.*, Barrett et al., 2004; Poage et al., 2008). The majority of samples had NH_4^+ concentration below detection except for plots 01, 09, 10, 22, 31, 33. Soil organic carbon and total nitrogen concentrations were higher than average compared to soils in this part of Taylor Valley (Barrett et al., 2006b, 2007) and may reflect the influence of moderate to dense biocrusts found in our most productive plots (Table 2). Importantly, dense biocrust plot 09 had the lowest electrical conductivity (indicator of soils that are regularly flushed by water), a more neutral pH, and a relatively higher concentration of ammonium, NH_4^+, (indicative of active microbial decomposition). Moreover, plot 09 had more than 5*x* the AFDM of the other plots on average. In a PCA on correlation, plot types are not significantly distinguished by physico-chemical properties (MANOVA, p-value = 0.56) (Fig. S3). However, NH_4^+ availability is significantly different among the plot types (ANOVA, p-value = 0.044) with dense biocrust most associated with increasing NH_4^+ availability.

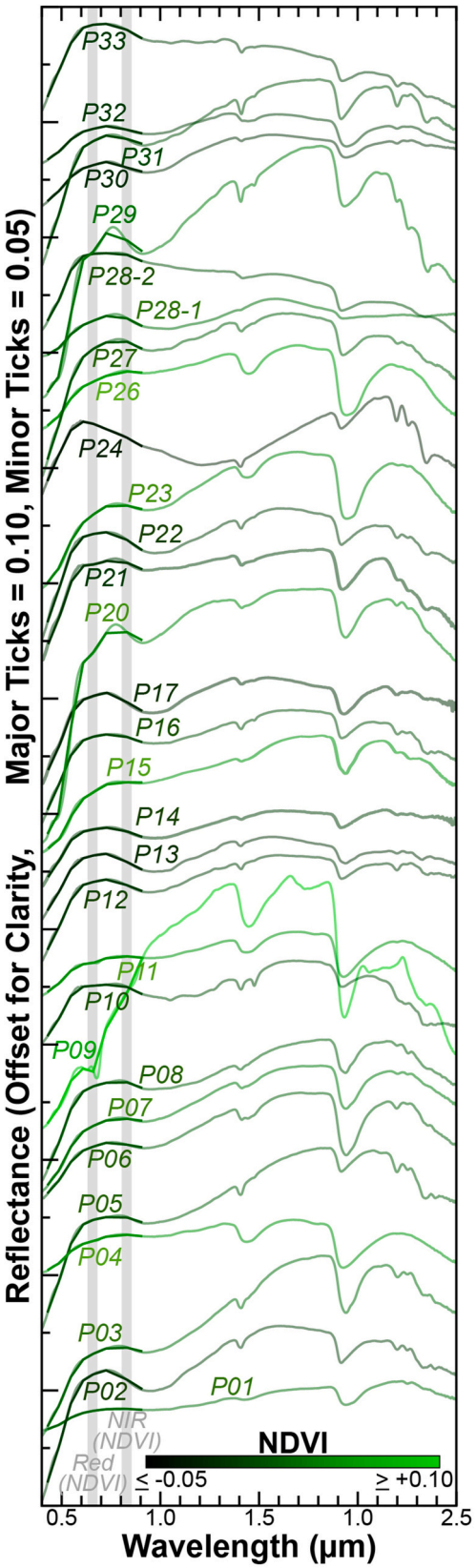

Fig. 6. Spectra acquired from each plot's surface soil or biocrust sample using a hyperspectral imaging spectrometer. Spectra downsampled to WV-2 resolution are shown in bold in the NDVI identified region of the spectrum with gray bars. Bright green spectra indicate higher NDVI. (For interpretation of the references to color in this figure legend, the reader is referred to the Web version of this article.)

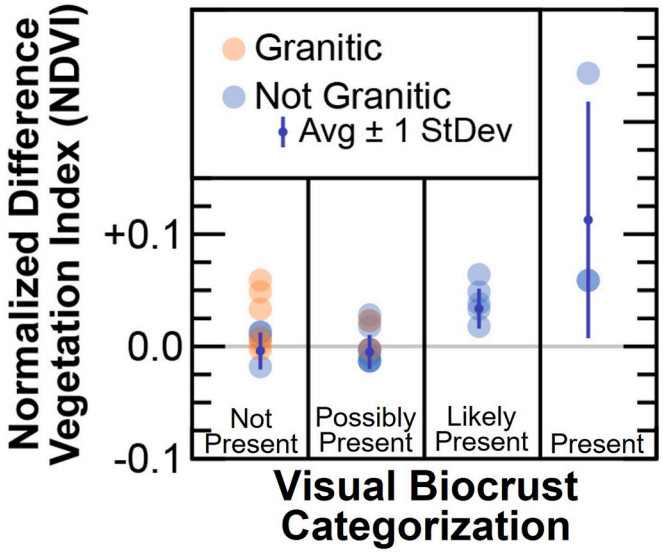

Fig. 7. Confidence in biocrust presence at each plot location, based on human interpretation in the field, compared to hyperspectral NDVI measurements acquired from samples transferred to and measured in the laboratory. Visually identified oxidized granite dominated plots are denoted in orange and the remaining plots (biocrust or typical soil) are denoted in blue. (For interpretation of the references to color in this figure legend, the reader is referred to the Web version of this article.)

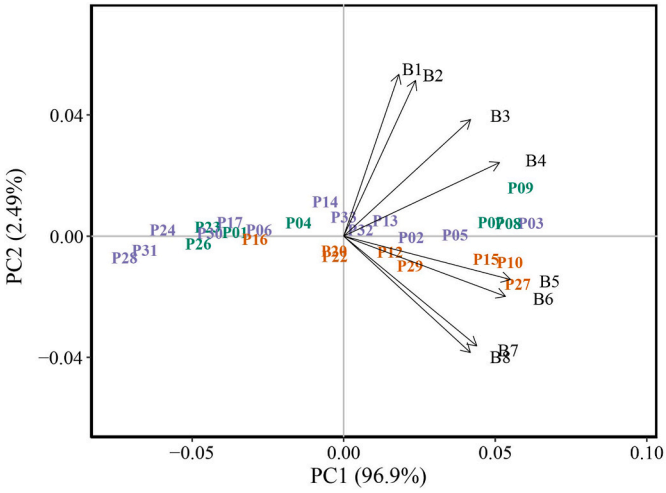

Fig. 8. Principal components analysis ordination on covariance of 28 plots (2 plots excluded due to snow coverage). Plots with ground cover consisting mainly of oxidized granite are shown in orange, biocrust and incipient biocrust in green, and typical soil in purple. Plots shown in green are categorized as biocrust "present" or "likely present" based on our visual biocrust categorization. Vectors represent correlations of WorldView-2 band reflectance (B1 – B8) with PCA ordination axes (all displayed correlations are significant, $p < 0.001$). Spectral data were acquired by the WV-2 satellite on Dec 03, 2019. (For interpretation of the references to color in this figure legend, the reader is referred to the Web version of this article.)

3.4. Spectral linear unmixing of orbital data

The linear spectral unmixing analysis of an early season (Dec 21, 2021) and late season (Jan 21, 2015) image demonstrated consistency in surface cover estimates between the two images (Table 3). RMSE were relatively low except for areas that were snow covered (*i.e.*, also displayed high albedo values). Notably, these snowy areas often coincided with plots that were identified in the field as either having biocrust

Table 1
Biological variables averaged (n = 5) ± 1 standard deviation from each of the 12 intensively sampled plots. Invertebrates are counted as the number of total-living.

Plot ID	AFDM (mg cm^{-2})	Chlorophyll (μg cm^{-2})	Carotenoid (μg cm^{-2})	Scytonemin (μg cm^{-2})	Nematodes (# kg^{-1} dry soil)	Rotifers (# kg^{-1} dry soil)	Tardigrades (# kg^{-1} dry soil)
P01	5.35	0.009	0.062	0.864	362	0	2
	±2.81	±0.006	±0.030	±0.693	±804	±0	±5
P09	28.29	4.974	2.141	77.395	1102	30	1822
	±21.62	±5.698	±2.500	±89.278	±735	±38	±2144
P10	2.12	0.007	0.031	0.331	1453	32	2
	±0.49	±0.002	±0.009	±0.109	±1405	±31	±4
P14	4.06	0.006	0.063	0.800	959	0	0
	±1.06	±0.006	±0.030	±0.314	±1990	±0	±0
P17	3.90	0.005	0.040	0.683	449	0	0
	±0.79	±0.003	±0.016	±0.231	±756	±0	±0
P22	2.19	0.005	0.027	0.285	0	0	0
	±0.95	±0.002	±0.004	±0.049	±0	±0	±0
P23	2.99	0.002	0.040	0.399	85	0	0
	±0.89	±0.002	±0.026	±0.271	±179	±0	±0
P27	3.18	0.006	0.032	0.432	168	0	0
	±1.12	±0.003	±0.013	±0.186	±354	±0	±0
P28	2.55	0.003	0.033	0.379	495	2	0
	±0.51	±0.002	±0.017	±0.165	±595	±5	±0
P30	3.46	0.005	0.036	0.272	0	0	0
	±0.57	±0.003	±0.023	±0.184	±0	±0	±0
P31	3.87	0.007	0.037	0.309	0	0	0
	±0.77	±0.002	±0.013	±0.122	±0	±0	±0
P33	2.61	0.004	0.019	0.137	875	0	0
	±0.84	±0.003	±0.003	±0.054	±1288	±0	±0

Table 2
Physical and chemical variables averaged (n = 5) ± 1 standard deviation from each of the 12 intensively sampled plots where "GWC" refers to gravimetric water content, "EC" electrical conductivity, "TOC" total organic carbon, and "TN" total nitrogen.

Plot ID	GWC (g/g)	EC (μS cm^{-1})	pH	NH_4^+	NO_3^-	PO_4^{3-}	TOC	TN
				μg N g^{-1} dry soil	μg N g^{-1} dry soil	μg P g^{-1} dry soil	mg C g^{-1} dry soil	mg N g^{-1} dry soil
P01	0.06	2330	8.4	0.12	57.87	3.56	0.309	0.112
	±0.03	±2318	±1.3	±0.19	±60.82	±0.54	±0.08	±0.05
P09	0.06	70	8.5	0.09	0.86	3.12	1.24	0.176
	±0.04	±37	±0.7	±0.19	±0.36	±0.66	±0.34	±0.04
P10	0.02	112	9.9	0.02	0.002	4.47	0.405	0.119
	±0.00	±50	±0.4	±0.04	±0.01	±5.93	±0.08	±0.04
P14	0.06	2311	8.6	0	48.30	12.19	1.14	0.203
	±0.02	±1819	±0.7	±0	±43.83	±6.15	±0.55	±0.07
P17	0.02	1095	8.8	0	65.79	5.85	0.497	0.115
	±0.01	±654	±0.5	±0	±71.17	±2.65	±0.19	±0.04
P22	0.05	2152	9.5	0.02	65.51	18.65	1.11	0.178
	±0.02	±786	±0.6	±0.03	±51.13	±10.70	±0.58	±0.06
P23	0.02	907	9.6	0	13.43	3.34	0.272	0.081
	±0.01	±283	±0.6	±0	±7.04	±0.40	±0.07	±0.02
P27	0.03	656	8.4	0	4.32	2.71	0.495	0.097
	±0.04	±523	±0.3	±0	±5.95	±1.07	±0.16	±0.02
P28	0.08	515	8.9	0	5.17	3.00	0.529	0.099
	±0.09	±440	±0.5	±0	±7.02	±2.03	±0.28	±0.02
P30	0.04	2347	9.0	0	33.40	3.70	0.364	0.111
	±0.03	±2602	±0.8	±0	±46.07	±1.70	±0.21	±0.06
P31	0.05	2431	8.2	0.01	27.68	1.70	0.275	0.074
	±0.02	±1757	±0.3	±0.01	±22.36	±0.52	±0.09	±0.02
P33	0.02	130	9.6	0.03	0.12	2.30	0.352	0.085
	±0.00	±67	±0.3	±0.05	±0.27	±0.88	±0.11	±0.02

present or likely present (incipient biocrust). Half of locations with biocrust or incipient biocrust (n = 4 of 8) were snow covered during the early season image. The remaining locations with biocrust and incipient biocrust were all within 15–35 m of snowpacks, measured from the center of the plots. Among the remaining 22 plots identified as biocrust not present or possibly present, only 3 plots contained some pixels with RMSE >0.5%. One of these plots contained some snow cover and lacked visible biocrust (P33), while the other two plots did not contain snow cover in the immediate area (P29, 30). Table 3 includes a subset of our 30 plots documenting the consistency of surface cover types between our two analyzed images, and also demonstrates the likely association between the presence of biocrust and snow cover.

3.5. Albedo analysis of orbital data

To identify any possible associations between biocrust cover and early season snowpack, the mean albedo and albedo SD were calculated for all plots among several December and January images (Fig. 9). Locations that contained snow cover had greater mean albedo, primarily early in the season when snowpacks are most present, and greater albedo SD between images based on the seasonality of snow and surface soil moisture. All of the plots that contained visually conspicuous biocrust cover had higher mean albedo and albedo SD than typical soil or oxidized granite plots. While not *all* of our biocrust identified plots were associated with variations in snow cover within the immediate area of

Table 3
Modeled abundance of total biocrust, oxidized granite, and remaining abiotic endmembers at a select number of plots visually identified by the surface type. 'Other abiotic' is the combination of the soil and water endmember abundances. An 'early season' and a 'late season' WV-2 image were selected for the spectral linear unmixing: Dec 21, 2021 and Jan 21, 2015, respectively. Specific pixels were excluded from the abundance average (n = 25 per plot) if the RMSE >0.5%, common for snow covered areas.

Plot ID	Surface Type Visually Present	Dec 21, 2021 'Early Season'					Jan 21, 2015 'Late Season'				
		Modeled Abundance (%)			Average % RMSE	% Excluded Pixels	Modeled Abundance (%)			Average % RMSE	% Excluded Pixels
		Biocrust	Oxidized Granite	Other Abiotic			Biocrust	Oxidized Granite	Other Abiotic		
P02	soil	0.6	2.4	97.0	0.302	0	1.7	9.4	88.9	0.240	0
P04	biocrust	–	–	–	5.000	100	8.4	11.0	80.6	0.260	0
P09	biocrust	–	–	–	5.863	100	16.5	11.3	72.2	0.200	0
P10	oxidized granite	9.5	39.9	50.6	0.181	0	2.5	52.1	45.3	0.150	0
P11	biocrust	–	–	–	5.297	100	4.2	1.7	94.1	0.190	0
P14	soil	0.6	4.9	94.4	0.303	0	0.4	5.5	94.1	0.260	0
P17	soil	2.7	6.9	90.4	0.309	0	1.3	12.0	86.7	0.220	0
P20	oxidized granite	7.4	50.2	42.4	0.203	0	1.9	49.6	48.4	0.170	0
P22	oxidized granite	5.8	40.2	54.0	0.160	0	2.1	69.4	28.6	0.170	0
P23	incipient biocrust	0.4	23.5	76.0	0.226	0	0.0	33.9	66.1	0.220	0
P26	incipient biocrust	7.7	29.1	63.2	0.201	0	12.2	1.0	86.8	0.241	0
P27	oxidized granite	2.2	27.0	70.9	0.168	0	4.3	20.9	74.8	0.224	0
P29	oxidized granite	16.7	39.3	44.0	0.308	24	17.8	39.3	42.9	0.303	16
P30	soil	3.5	25.8	70.8	0.226	4	0.8	24.4	74.8	0.262	0
P31	soil	7.6	25.8	66.6	0.231	0	3.3	8.9	87.7	0.276	0

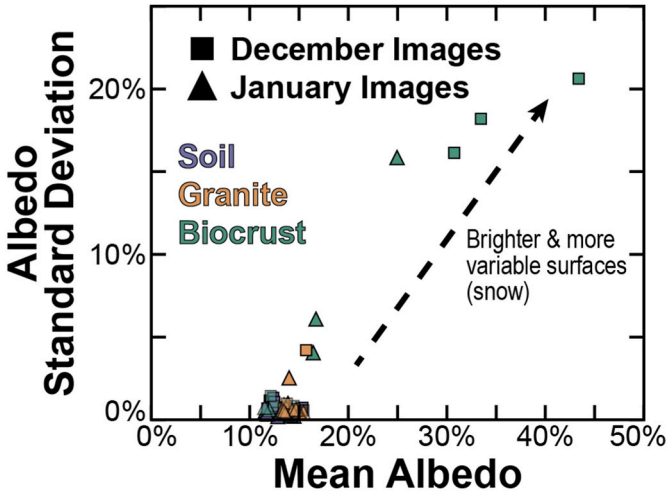

Fig. 9. Mean and standard deviation albedo of early season December and late season January WorldView-2 and -3 images at each of the 30 plots locations. Colors indicate surface type of plot. Biocrust plots include those which were identified in the field as having visually conspicuous biocrust present or likely present (incipient biocrust). (For interpretation of the references to color in this figure legend, the reader is referred to the Web version of this article.)

the plots (note that biocrust can obtain moisture from groundwater seeps or melting subsurface ice as well), we do find that the brightest and most variable surfaces in our study area are all biocrust identified areas (Fig. 9).

4. Discussion

4.1. Laboratory spectral detection of biocrust

Our laboratory spectral validation study demonstrated that biocrust present in soil microcosms is detectable at abundances as low as 1% by weight, and that spectral linear unmixing models can be used to successfully predict biocrust abundance. The absorption feature associated with photosynthetic pigments (~0.68 μm) is present in all biocrust microcosm mixtures, including the 1% biocrust microcosm where the feature is observable as well (Fig. 3). When comparing the modeled biocrust abundance of each sample mixture to the actual measured biocrust abundance, there is a strong linear fit between the modeled and measured abundance with an R^2 of 0.99 (Fig. 4). We have shown how, under ideal conditions, mixtures of biocrust and soil combine linearly in VNIR spectral space, allowing for linear unmixing models to accurately predict biocrust abundance. This detection method is successful over a range of abundances analogous to dense microbial mat communities associated with productive aquatic habitats (Power et al., 2020; Salvatore et al., 2021) and sparse biocrusts in the more typical arid soils of the MDV. Despite the known complexities associated with extrapolating these results to field and orbital data (*e.g.*, atmospheric contributions, variations in biotic and abiotic surface composition and moisture), the relationships derived in our laboratory analyses are successful in identifying and quantifying biocrust and can be modeled to approximate the distribution of microbial communities in the MDV.

4.2. Oxidized granite impedes use of vegetation indices

It was evident during our field surveying and sampling campaign that geological features are a significant factor in the detection of low density biocrusts in dry terrestrial environments. While the soils and dominant lithologies of the MDV have been widely characterized by previous investigators (*e.g.*, Bockheim et al., 2008), isolated outcrops or boulders of distinct composition have been shown to locally influence observed spectral signatures. For example, during our field campaign, several plots with high NDVI values were found to be predominantly covered by oxidized granitic boulders (Fig. 5 e, h). Despite their high NDVI values, these oxidized granite plots lack visible biocrust presence based on visual observation in the field (Fig. 7) and had low AFDM and chlorophyll contents (Table 1), indicating that these relatively high NDVI values are not associated with photosynthesis. The hyperspectral data of the surface samples of all plots illustrated clear distinctions among the plots (Fig. 6). For example, plots 20 and 29 were located within oxidized granite boulder fields and exhibit two broad absorption features associated with the presence of ferrous and ferric iron (Fe), centered near 0.67 μm and 0.94 μm, and resulting in a broad reflectance peak at approximately 0.74 μm (Fig. 5 k; Fig. S2). While the hyperspectral shape of these granitic spectra is distinct from those of biocrust, NDVI does not effectively distinguish between them due to the granitic spectra containing an Fe-absorption feature at red wavelengths and thus

Table 4
Continuum of hydrological conditions in Taylor Valley, Antarctica.

Landscape Feature	Water Abundance	Salinity	Biological Activity
Arid Terrestrial Landscape	Low	Low-High	Low
Hypersaline Water Tracks	Medium	High	Low
Snowpack-Fed Microhabitats	Low-Medium	Low-Medium	Medium
Snowpack-Fed Non-Annual Ephemeral Wetlands	Medium	Low-Medium	Medium
Annual Ephemeral Streams	Medium-High	Low	Medium-High
Lakes	High	Low	High

an increase in reflectance in the NIR (Fig. S2). This change in reflectance creates a slope that causes these granitic areas to have a high NDVI, despite not being correlated to indicators of photosynthetic activity (*e.g.*, chlorophyll or AFDM). While hyperspectral reflectance data can be used to distinguish these abiotic absorption features from those associated with biological activity, simple multispectral parameters (*e.g.*, NDVI) are less capable of distinguishing between these different compositions and are therefore less reliable at detecting biocrust presence.

4.3. Biocrust distribution is associated with seasonal snowpacks

In contrast to soils with oxidized granites, several locations contained sparse, incipient biocrust, where it appeared that cyanobacteria colonies and potentially moss were emerging from wet desert pavement (Fig. 1 c). The locations identified as having biocrust present or likely present had relatively higher NDVI compared to the desert pavement locations not containing biocrust and which upon analyses were shown to have low chlorophyll concentrations and AFDM. Of particular interest, plot 09 hosted dense biocrust (Fig. 5 d, g) and diverse soil fauna (Table 1), similar in composition to the diversity found near stream and lake ecosystems (Ayres et al., 2007; Treonis et al., 1999). Plot 09 is outside of any stream channel or water track and is ~700 m above the current elevation of Lake Fryxell. The only visible source of liquid water for plot 09 are a series of snowpacks immediately uphill and ~10 and 50 m uphill (at the time of sampling and visible in multiple satellite images). While diverse invertebrate communities are common near aquatic environments in the Fryxell basin (Courtright et al., 2001; Freckman and Virginia, 1997), they have not been commonly reported for upland soils outside stream channels.

One well-documented landscape that exhibits similar biotic diversity to plot 09 is the Wormherder Creek wetland in western Taylor Valley on the south side of the west lobe of Lake Bonney (Harris et al., 2007; Simmons et al., 2009b; Nielsen et al., 2012). Unlike the soil biocrusts documented here (*e.g.*, plot 09), which are fed by the melt of relatively small snowpacks (<60 m in diameter), the Wormherder Creek wetland is fed intermittently by the melt of large snowpacks on the southern valley wall which create melt-water drainages that have contributed to saturated soils and overland flow on at least 3 documented occasions (sufficiently warm and sunny summers) in the last thirty years (Lyons et al., 2005; Nielsen et al., 2012; Wlostowski et al., 2019; Stanish et al., 2012; Harris et al., 2007). Abundant microbial mats hosting diatom and invertebrate communities have been described in Wormherder Creek (Nielsen et al., 2012; Stanish et al., 2012; Simmons et al., 2009b). Both these snowpack-fed meltwater environments are examples of biological hotspots in an otherwise arid terrestrial landscape physically separated from the diverse communities within the annual ephemeral streams.

These snowpack-fed biological hotspots are distinct from the water track features described by Levy et al. (2011), which are narrow areas of subsurface hydrologic flow that route water downslope through soils above the ice table and lack overland flow. Water tracks are more saline in comparison to the surrounding landscape and therefore do not host conspicuous surface biocrust, microbial mats, or invertebrate communities (Kuentz et al., 2022; Levy et al., 2011, 2014). Therefore, biological activity in these snowpack areas is not driven solely by the presence of liquid water, but also suitable soil conditions as well.

A continuum of hydrological conditions exists: the arid terrestrial landscape, hypersaline water tracks, snowpack-fed microhabitats, snowpack-fed non-annual ephemeral wetlands, annual ephemeral streams, and lakes (Table 4). Plot 09 is compositionally and chemically more similar to near-stream environments than to the persistently dry and low organic matter soils that characterize most of this arid terrestrial landscape (Burkins et al., 2001; Barrett et al., 2006a). For example, plot 09 is wetter and less alkaline than the other soil plots with low or no biocrusts, which are representative of the arid soils described by Barrett et al. (2006a) and Campbell et al. (1998) (Table 2). Plot 09 also has the lowest electrical conductivity, which is an indicator that soils are regularly flushed by water, and it has a relatively higher concentration of ammonium, NH_4^+, typical for biologically active soils with active turnover of organic matter (Barrett et al., 2009). Additionally, the concentration of soil organic C in this plot is more than 2x greater on average than previous reports for arid soils in Taylor Valley (Barrett et al., 2006b; Burkins et al., 2001) and closer to the concentrations of C in near-stream and lake sediments (Barrett et al., 2009). Moreover, the mass of carbon in the biocrust itself is 2–3x greater than that in the underlying surface soils (Burkins et al., 2001), indicating the importance of including biocrust estimates in regional carbon mass balances. Rather than viewing this landscape as simply aquatic or terrestrial units, a continuum of hydrological conditions exists, and these snowpack-fed landscapes constitute a unique component of the soil-sediment environment. Elucidating the factors contributing to the structure and function of these snowpack-associated environments is essential for refining our understanding of species distribution and organic C balance in the MDV.

4.4. Comparisons between multispectral and hyperspectral data

There are inherent limitations to multispectral data when they are used for detecting surfaces that are spectrally weaker and discontinuous, such as patchy biocrusts. When investigating our intensively sampled plots which had *in-situ* biological data collected (*i.e.*, AFDM, pigment content), there were no significant correlations between the biological parameters and multispectral vegetation indices and raw bands (Table S2). There were some correlations (*e.g.*, with B1, R ~ 0.73; and with B2, R ~ 0.64) that were driven by plot 09 with orders of magnitude higher AFDM and pigment concentration, but all significant correlations were lost when removing this dominant plot. Solely using these traditional multispectral indices is inadequate for identifying patchy biocrust surfaces, specifically in areas with spectrally dominant surface geology, such as the MDV.

Hyperspectral reflectance measurements were essential in this study to understand the spectral complexities of our surface types. For example, plot 09 contained the most visibly dense biocrust in our field campaign and was spectrally unique with the highest NDVI measured from hyperspectral data in the laboratory (Fig. 6). However, it did not always have the highest satellite-derived NDVI as expected; the oxidized granite areas sometimes had higher NDVI across images. This demonstrates the differences in spectral resolution between a hyperspectral reflectance spectrometer and a multispectral satellite, and also the differences in surface area of larger granitic surfaces compared to patchy biocrust surfaces when using satellite data. Additionally, this difference

in plot 09 NDVI from hyperspectral laboratory measurements to multispectral orbital data could also in part be the result of fluctuating biological activity through time. For example, a 2019 WorldView-3 image shows higher NDVI at this location in January when the snow generally melts, the surrounding soils are moist, and the biocrust communities are likely active (Fig. 5 a). Barták et al. (2016) and Trnková and Barták (2017) both demonstrate the relationship between water content in black microbial mats, their photosynthetic activity, and their resultant spectral signatures. Their results indicate that there is a reduction in NDVI by roughly 50% from maximum photosynthetic signatures at roughly 55% relative water content (RWC) to complete desiccation at 0% RWC. These and other authors (*e.g.*, Salvatore et al., 2021) also note how burial by windblown sand can significantly mask the spectral signatures of dry mats and biocrusts. Together, these studies and our results demonstrate there are many factors that can influence the observed NDVI signature at multispectral resolutions beyond simply the abundance of photosynthetic biomass, and hyperspectral data were necessary to elucidate these interactions.

However, incorporating all multispectral bands makes it possible to differentiate between the three plot types here (Fig. 8). The gradient of plots from bare soil to denser biocrust along the raw WV-2 band reflectance vectors informs a detection threshold for biocrust around 47% cover or 280 g m^{-2} AFDM (plot 09). The oxidized granite plots are most spectrally dissimilar from the biocrust and soil plots. When using the vegetation indices calculated from the multispectral data, it is also possible to statistically distinguish among plot types. Though, the plots with the highest vegetation index values are those with the oxidized granite surfaces. It is evident through our analyses that surface geology in this environment can result in higher NDVI values, which is not indicative of biological activity, but are instead spectrally dominant areas in the wavelengths typically diagnostic for photosynthesis. Although hyperspectral data in the laboratory show that biocrust is identifiable and distinct from oxidized granite surfaces and typical soil surfaces, we are currently limited to multispectral resolution with available satellite data. While vegetation indices are also limited in the number of bands they incorporate and are shown here to be affected by surface geology, incorporating all eight multispectral bands proves useful in distinguishing biologically active surfaces. It is of particular importance to note that the overall success of our analyses was dependent on our ability to ground truth, which allows us to confidently link spectral data to what we saw and measured with boots on the ground.

4.5. Spectral linear unmixing models predict biocrust abundance

Moving beyond traditional remote sensing indices, we applied spectral linear unmixing models to WV-2 orbital data using spectral endmembers collected from the field with a hyperspectral reflectance spectrometer, including an oxidized granite endmember (Table 3). The low RMSE associated with the unmixing of all surface types discussed here demonstrates that there are no clearly omitted spectral endmembers. Although our hyperspectral measurements outperform multispectral data in terms of biological detection, we are limited to multispectral bands with available satellite imagery. However, using multispectral orbital data, our results demonstrate how linear unmixing models perform better than vegetation indices, because they use all eight multispectral bands as opposed to only a few select bands. Specifically, there are clear spectral differences between oxidized granites and photosynthetic biocrust when all eight spectral bands are investigated, but these differences are lost when using vegetation parameters like NDVI. While some endmembers are less spectrally unique at multispectral resolutions in comparison to hyperspectral and can confuse the unmixing models at times, these models are still a far improvement over simple vegetation indices in detecting low density biocrusts and can be used to infer ecologically relevant properties of biocrust in this region. Most notably, our unmixing analyses with RMSE indicate that plots containing biocrust were all either snow covered or within 15–35 m of snowpacks during an early season (Dec 21, 2021) WorldView-2 image (Table 3). This result suggests snowpacks are important sources of moisture sustaining biocrust community microhabitats in an otherwise arid terrestrial landscape, and therefore encourages further investigation.

4.6. Snowpacks as microhabitats for biocrusts and diverse soil communities

To identify associations between biocrust cover and early season snowpack, we visualized the mean albedo and albedo SD for all plots based on surface type among several December and January images (Table S1). We found that the brightest and most variable surface areas, where snow is present, were areas that were identified as biocrust visually in the field (Fig. 9). There are biocrust areas that have lower mean and SD albedo and are likely associated with other sources of moisture, like groundwater seeps or snow, which accumulates to a much lesser extent and melts earlier in the season. Among our plots, the highest and most variable albedo surfaces are associated with biocrust presence, indicating that these MDV biocrust habitats are likely associated with areas where snow accumulates early in the season, slowly melts later in the season, and supplies soil communities and biocrusts with sufficient moisture to sustain biological activity throughout the austral summers.

Snow is an important surface component of the Taylor Valley. Seasonal snow accumulates more on the eastern portion of the Taylor Valley closer to the coast (Eveland et al., 2012, 2013; Fountain et al., 2010). The Fryxell basin, where our study region is located, receives the greatest annual snowfall and has the highest interannual variability of snowfall within Taylor Valley (Myers et al., 2022). The Fryxell basin region received an average of 11.5 mm wet equivalent of snow accumulation from 1995 to 2017 between the months of August and May (Myers et al., 2022). While the magnitude of snowfall and snow accumulation is dependent on the variability of the frequency and intensity of storms and winds, snow is expected to collect in the same locations inter-annually because snow accumulation is most associated with variation in fine-scale topography (Eveland et al., 2012, 2013). Seasonal snow accumulates across a large portion of the Fryxell basin region. For example, prior research has shown accumulation covering an area of 10.29 km^2 (17.83% of the Fryxell basin delineated region) in late October of 2009 (Eveland et al., 2012). By mid-January of 2010, 93% of the snow accumulation was lost (Eveland et al., 2012), primarily due to sublimation given the arid environment but also due to snowmelt. For example, Gooseff et al. (2003) and Ayres et al. (2010) observed increases in soil moisture near snowpacks compared to the nearby dry soils. Eveland et al. (2012) also suggest that volumes of water that usually seem insignificant to some ecosystems may be an important driver in structuring communities below snow in highly water-limited environments such as the MDV. Snow cover has also been shown to reduce temperature extremes in underlying soil and influence biogeochemical cycling and microbial activity in soils generally (Schimel et al., 2004; Van Horn et al., 2013).

Furthermore, we suggest that snowpacks commonly occurring throughout eastern Taylor Valley provide enough moisture for the development of biocrusts and underlying soil communities and likely create suitable microhabitats shielded from temperature extremes and intense UV-radiation. Given the broader spatial extent of the terrestrial landscape outside of stream channels and lake margins and the abundance of snowpacks, we anticipate that a considerable proportion of the valley-wide carbon budget is represented by biocrust communities. To refine the Taylor Valley carbon budget, future field work should incorporate more sampling and surveying of these snowpack areas to document the influence of snowpack variability on the dynamics of biocrust and soil microbial communities in the MDV. Given the strong interannual variability of snowfall and snow persistence in the Taylor Valley (Myers et al., 2022), the documented occurrence of anomalous weather events (Barrett et al., in review), and the prediction that Antarctic coasts

will experience more frequent and intense rainfall by the end of the century (Vignon et al., 2021), we encourage continued research on these biocrust microhabitats in this currently water-limited but increasingly dynamic landscape.

5. Conclusion

Here, we show that low density biocrusts are patchily distributed throughout the eastern Taylor Valley region in upland areas away from streams and lake margins. Seasonal snowpacks create microhabitats for these biocrust communities to successfully thrive in this otherwise harsh, desert environment. Soils beneath these biocrusts can support diverse soil fauna, similar in community composition to soils immediately beside streams and lake margins. A continuum exists between aquatic and terrestrial environments where microhabitats are driven by snowpacks physically separate from streams that otherwise have ecosystem properties and biological diversity more similar to the local streams than the nearby arid soils. We suggest that these snowpack-fed microhabitats are unique ecosystems and a key ecological component to the region's carbon budget. Moreover, our work to study these microhabitats in further detail is ongoing (*e.g.*, Power et al., *in prep*), and we encourage other efforts as well.

Ground truthing is essential for detecting and mapping biocrust. Although geological surface composition can impede use of NDVI on soils, spectral linear unmixing methods are a practical alternative for successful biocrust detection. Our modeling efforts are currently the foundation of follow-up studies where further validation efforts in the field are needed to extrapolate the model and test our hypotheses about hydrological transitions and their influence on photoautotrophic communities. This work brings us closer in our efforts to refine the carbon budget for this region and to examine the controls over the distribution and activity of these critical soil communities. These remote sensing technologies are ideal for measuring ecosystem dynamics in Antarctic ecosystems, which are particularly climate-sensitive and difficult to access.

Funding

This work was supported by the National Science Foundation (NSF) through grants #1637708 and #2224760 to the McMurdo Dry Valleys Long Term Ecological Research Project; NSF through grant #1745053 to M. Salvatore, J. Barrett, and grant #1744849 to E. Sokol, L. Stanish; and the Virginia Space Grant Consortium 2020–2021 and 2021–2022 Fellowship Programs to S. Power.

CRediT authorship contribution statement

Sarah N. Power: Conceptualization, Data curation, Formal analysis, Investigation, Methodology, Visualization, Writing – original draft, Writing – review & editing, Software. **Mark R. Salvatore:** Conceptualization, Data curation, Formal analysis, Funding acquisition, Investigation, Methodology, Resources, Supervision, Visualization, Writing – review & editing, Software. **Eric R. Sokol:** Conceptualization, Funding acquisition, Writing – review & editing. **Lee F. Stanish:** Conceptualization, Funding acquisition, Writing – review & editing. **Schuyler R. Borges:** Conceptualization, Writing – review & editing. **Byron J. Adams:** Funding acquisition, Investigation, Resources, Writing – review & editing, Methodology. **J.E. Barrett:** Conceptualization, Funding acquisition, Methodology, Resources, Supervision, Writing – review & editing, Formal analysis.

Declaration of competing interest

The authors declare that they have no known competing financial interests or personal relationships that could have appeared to influence the work reported in this paper.

Data availability

All data presented in this study are archived in the Environmental Data Initiative (EDI) Data Repository (Power et al. 2023).

Acknowledgements

We would like to acknowledge the Polar Geospatial Center for geospatial support and DigitalGlobe, Inc. for access to satellite imagery. We appreciate Antarctic Support Contractors and Air Center Helicopters for providing operational support in the field. We would also like to thank Ernest Osburn for assistance with ground truthing and sample collection in the field, and Bobbie Niederlehner and Maxwell Craddock for their assistance with laboratory analyses. Additionally, we acknowledge the two anonymous reviewers whose thoughtful feedback improved the clarity and organization of this manuscript.

Appendix A. Supplementary data

Supplementary data to this article can be found online at https://doi.org/10.1016/j.srs.2024.100120.

References

Adams, J.B., Smith, M.O., Gillespie, A.R., 1993. In: Imaging spectroscopy: interpretation based on spectral mixture analysis. In: Remote Geochemical Analysis: Elemental and Mineralogical Composition. Cambridge Univ. Press, New York, pp. 145–166.

Adams, B.J., Bardgett, R.D., Ayres, E., Wall, D.H., Aislabie, J., Bamforth, S., Bargagli, R., Cary, C., Cavacini, P., Connell, L., Convey, P., Fell, J.W., Frati, F., Hogg, I.D., Newsham, K.K., O'Donnell, A., Russell, N., Seppelt, R.D., Stevens, M.I., 2006. Diversity and distribution of Victoria land biota. Soil Biol. Biochem. 38, 3003–3018. https://doi.org/10.1016/J.SOILBIO.2006.04.030.

Alger, A.S., McKnight, D.M., Spalding, S.A., Tate, C.M., Shupe, G.H., Welch, K.A., Edwards, R., Andrews, E.D., House, H.R., 1997. Ecological Processes in a Cold Desert Ecosystem: the Abundance and Species Distribution of Algal Mats in Glacial Meltwater Streams in Taylor Valley, Antarctica. Institute of Arctic and Alpine Research Occasional. Paper 51.

Ayres, E., Wall, D.H., Adams, B.J., Barrett, J.E., Virginia, R.A., 2007. Unique similarity of faunal communities across aquatic–terrestrial Interfaces in a polar desert ecosystem. Ecosystems 10, 523–535. https://doi.org/10.1007/s10021-007-9035-x.

Ayres, E., Nkem, J.N., Wall, D.H., Adams, B.J., Barrett, J.E., Simmons, B.L., Virginia, R. A., Fountain, A.G., 2010. Experimentally increased snow accumulation alters soil moisture and animal community structure in a polar desert. Polar Biol. 33, 897–907. https://doi.org/10.1007/s00300-010-0766-3.

Barrett, J.E., Virginia, R.A., Wall, D.H., Parsons, A.N., Burkins, M.B., 2004. Variation in biogeochemistry and soil biodiversity across spatial scales in a polar desert ecosystem. Ecology 85, 3105–3118. https://doi.org/10.1890/03-0213.

Barrett, J.E., Virginia, R.A., Hopkins, D.W., Aislabie, J., Bargagli, R., Bockheim, J.G., Campbell, I.B., Lyons, W.B., Moorhead, D.L., Nkem, J.N., Sletten, R.S., Steltzer, H., Wall, D.H., Wallenstein, M.D., 2006a. Terrestrial ecosystem processes of victoria land, Antarctica. Soil Biol. Biochem. 38, 3019–3034. https://doi.org/10.1016/J.SOILBIO.2006.04.041.

Barrett, J.E., Virginia, R.A., Parsons, A.N., Wall, D.H., 2006b. Soil carbon turnover in the McMurdo dry valleys, Antarctica. Soil Biol. Biochem. 38, 3065–3082. https://doi.org/10.1016/j.soilbio.2006.03.025.

Barrett, J.E., Virginia, R.A., Wall, D.H., Cary, S.C., Adams, B.J., Hacker, A.L., Aislabie, J. M., 2006c. Co-variation in soil biodiversity and biogeochemistry in northern and southern Victoria Land, Antarctica. Antarct. Sci. 18, 535. https://doi.org/10.1017/S0954102006000587.

Barrett, J.E., Virginia, R.A., Lyons, W.B., McKnight, D.M., Priscu, J.C., Doran, P.T., Fountain, A.G., Wall, D.H., Moorhead, D.L., 2007. Biogeochemical stoichiometry of antarctic dry valley ecosystems. J. Geophys. Res. 112 https://doi.org/10.1029/2005JG000141.

Barrett, J.E., Adams, B.J., Doran, P.T., Dugan, H.A., Myers, K.F., Salvatore, M.R., Power, S.N., Snyder, M.D., Wright, A., Gooseff, M.N. In review. Weather whiplash in a terrestrial polar ecosystem following the March 2022 Antarctic weather anomaly.

Barrett, J.E., Gooseff, M.N., Takacs-Vesbach, C., 2009. Spatial variation in soil active-layer geochemistry across hydrologic margins in polar desert ecosystems. Hydrol. Earth Syst. Sci. Discuss. 6, 3725–3751. https://doi.org/10.5194/hessd-6-3725-2009.

Barták, M., Hazdrová, J., Skácelová, K., Hájek, J., 2016. Dehydration-induced responses of primary photosynthetic processes and spectral reflectance indices in Antarctic Nostoc commune. Czech Polar Rep 6, 87–95. https://doi.org/10.5817/cpr2016-1-9.

Belnap, J., 2003. The world at your feet: desert biological soil crusts. Front. Ecol. Environ. 1, 181–189. https://doi.org/10.1890/1540-9295(2003)001, 0181:TWAYFD]2.0.CO;2.

Belnap, J., Weber, B., Büdel, B., 2016. Biological soil crusts as an organizing principle in drylands. In: Weber, B., Büdel, B., Belnap, J. (Eds.), Biological Soil Crusts: an Organizing Principle in Drylands. Springer International Publishing, pp. 3–13.

Bioucas-Dias, J.M., Plaza, A., Dobigeon, N., Parente, M., Du, Q., Gader, P., Chanussot, J., 2012. Hyperspectral unmixing overview: geometrical, statistical, and sparse regression-based approaches. IEEE J. Sel. Top. Appl. Earth Obs. Rem. Sens. https://doi.org/10.1109/JSTARS.2012.2194696.

Bockheim, J.G., Prentice, M.L., McLeod, M., 2008. Distribution of glacial deposits, soils, and permafrost in Taylor Valley, Antarctica. Arctic Antarct. Alpine Res. 40, 279–286. https://doi.org/10.1657/1523-0430(06-057 [BOCKHEIM]2.0.CO;2.

Brenowitz, S., Castenholz, R.W., 1997. Long-term effects of UV and visible irradiance on natural populations of a scytonemin-containing cyanobacterium (Calothrix sp.). FEMS Microbiol. Ecol. 24, 343–352. https://doi.org/10.1016/S0168-6496(97)00075-5.

Burkins, M.B., Virginia, R.A., Wall, D.H., 2001. Organic carbon cycling in Taylor Valley, Antarctica: quantifying soil reservoirs and soil respiration. Global Change Biol. 7, 113–125. https://doi.org/10.1046/j.1365-2486.2001.00393.x.

Campbell, I.B., Claridge, G.G.C., Campbell, D.I., Balks, M.R., 1998. The soil environment of the McMurdo dry valleys, Antarctica. In: Ecosystem Dynamics in a Polar Desert: the Mcmurdo Dry Valleys, Antarctica, Antarctic Research Series. American Geophysical Union, Washington, D. C., pp. 297–322. https://doi.org/10.1029/ar072p0297

Cary, S.C., McDonald, I.R., Barrett, J.E., Cowan, D.A., 2010. On the rocks: the microbiology of Antarctic Dry Valley soils. Nat. Rev. Microbiol. 8, 129–138. https://doi.org/10.1038/nrmicro2281.

Couradeau, E., Karaoz, U., Lim, H.C., Nunes Da Rocha, U., Northen, T., Brodie, E., Garcia-Pichel, F., 2016. Bacteria increase arid-land soil surface temperature through the production of sunscreens. Nat. Commun. https://doi.org/10.1038/ncomms10373.

Courtright, E.M., Wall, D.H., Virginia, R.A., 2001. Determining habitat suitability for soil invertebrates in an extreme environment: the McMurdo Dry Valleys, Antarctica. Antarct. Sci. 13, 9–17. https://doi.org/10.1017/S0954102001000037.

Cox, S.C., Turnbull, I.M., Isaac, M.J., Townsend, D.B., Lyttle, B.S., 2012. Geology of Southern Victoria Land, Antarctica, vol. 1. Institute of Geological and Nuclear Sciences, p. 250, 000 Geological Map.

Doran, P.T., McKay, C.P., Clow, G.D., Dana, G.L., Fountain, A.G., Nylen, T., Lyons, W.B., 2002. Valley floor climate observations from the McMurdo dry valleys, Antarctica, 1986–2000. J. Geophys. Res. 107, 4772. https://doi.org/10.1029/2001JD002045.

Elbert, W., Weber, B., Burrows, S., Steinkamp, J., Büdel, B., Andreae, M.O., Pöschl, U., 2012. Contribution of cryptogamic covers to the global cycles of carbon and nitrogen. Nat. Geosci. 5, 459–462. https://doi.org/10.1038/ngeo1486.

Eveland, J., Gooseff, M.N., Lampkin, D.J., Barrett, J.E., Takacs-Vesbach, C., 2012. Spatial and temporal patterns of snow accumulation and aerial ablation across the McMurdo Dry Valleys, Antarctica. Hydrol. Process. 27 https://doi.org/10.1002/hyp.9407.

Eveland, J.W., Gooseff, M.N., Lampkin, D.J., Barrett, J.E., Takacs-Vesbach, C.D., 2013. Seasonal controls on snow distribution and aerial ablation at the snow-patch and landscape scales, McMurdo Dry Valleys, Antarctica. Cryosphere 7, 917–931. https://doi.org/10.5194/tc-7-917-2013.

Finger-Higgens, R., Duniway, M.C., Fick, S., Geiger, E.L., Hoover, D.L., Pfennigwerth, A. A., Van Scoyoc, M.W., Belnap, J., 2022. Decline in biological soil crust N-fixing lichens linked to increasing summertime temperatures. Proc. Natl. Acad. Sci. U.S.A. 119, e2120975119 https://doi.org/10.1073/pnas.2120975119.

Fountain, A.G., Nylen, T.H., Monaghan, A., Basagic, H.J., Bromwich, D., 2010. Snow in the McMurdo dry valleys, Antarctica. Int. J. Climatol. 30, 633–642. https://doi.org/10.1002/joc.1933.

Fountain, A.G., Fernandez-Diaz, J.C., Obryk, M., Levy, J., Gooseff, M., Van Horn, D.J., Morin, P., Shrestha, R., 2017. High-resolution elevation mapping of the McMurdo Dry Valleys, Antarctica, and surrounding regions. Earth Syst. Sci. Data 9, 435–443. https://doi.org/10.5194/essd-9-435-2017.

Freckman, D.W., Virginia, R.A., 1993. Extraction of nematodes from dry valley antarctic soils. Polar Biol. 13, 483–487. https://doi.org/10.1007/BF00233139.

Freckman, D.W., Virginia, R.A., 1997. Low-diversity antarctic soil nematode communities: distribution and response to disturbance. Ecology 78, 363–369. https://doi.org/10.1890/0012-9658(1997)078[0363:LDASNC]2.0.CO, 2.

Fritsen, C.H., Grue, A.M., Priscu, J.C., 2000. Distribution of organic carbon and nitrogen in surface soils in the McMurdo Dry Valleys, Antarctica. Polar Biol. 23, 121–128. https://doi.org/10.1007/s003000050017.

Garcia-Pichel, F., Castenholz, R.W., 1991. Characterization and biological implications of scytonemin, a cyanobacterial sheath. Pigment. J. Phycol. 27, 395–409. https://doi.org/10.1111/j.0022-3646.1991.00395.x.

Gooseff, M.N., Barrett, J.E., Doran, P.T., Fountain, A.G., Lyons, W.B., Parsons, A.N., Porazinska, D.L., Virginia, R.A., Wall, D.H., 2003. Snow-Patch influence on soil biogeochemical processes and invertebrate distribution in the McMurdo dry valleys, Antarctica. Arctic Antarct. Alpine Res. 35, 91–99. https://doi.org/10.1657/1523-0430(2003)035[0091:SPIOSB]2.0.CO;2.

Gooseff, M.N., Barrett, J.E., Levy, J.S., 2013. Shallow groundwater systems in a polar desert, McMurdo Dry Valleys, Antarctica. Hydrogeol. J. 21, 171–183. https://doi.org/10.1007/s10040-012-0926-3.

Harris, K.J., Carey, A.E., Berry Lyons, W., Welch, K.A., Fountain, A.G., 2007. Solute and isotope geochemistry of subsurface ice melt seeps in Taylor Valley, Antarctica. GSA Bulletin 119, 548–555. https://doi.org/10.1130/B25913.1.

Keeney, D.R., Nelson, D.W., 1982. Nitrogen—inorganic forms. In A.L. Page (ed.). Methods of soil analysis. Chemical and microbiological properties. Agronomy. Am. Soc. of Agron. 9 (2), 643–698. Madison, WI.

Knepel, K., 2003. Determination of nitrate in 2M KCl soil extracts by flow injection analysis. In: QuikChem Method 12-107-04-1-B. Lachat Instruments, Loveland, CO.

Kohler, T.J., Stanish, L.F., Crisp, S.W., Koch, J.C., Liptzin, D., Baeseman, J.L., McKnight, D.M., 2015. Life in the main channel: long-term hydrologic control of microbial mat abundance in McMurdo dry valley streams, Antarctica. Ecosystems 18, 310–327. https://doi.org/10.1007/s10021-014-9829-6.

Kuentz, L., Levy, J., Salvatore, M., 2022. Timing and duration of ephemeral Antarctic water tracks and wetlands using high temporal–resolution satellite imagery, high spatial–resolution satellite imagery, and ground-based sensors in the McMurdo Dry Valleys. Arctic Antarct. Alpine Res. 54, 538–561. https://doi.org/10.1080/15230430.2022.2123858.

Lawson, C.L., Hanson, R.J., 1974. Solving Least Squares Problems. Prentice-Hall, Englewood Cliffs, N.J.

Levy, J.S., 2013. How big are the McMurdo Dry Valleys? Estimating ice-free area using Landsat image data. Antarct. Sci. 25, 119–120. https://doi.org/10.1017/S0954102012000727.

Levy, J.S., Fountain, A.G., Gooseff, M.N., Welch, K.A., Lyons, W.B., 2011. Water tracks and permafrost in Taylor Valley, Antarctica: extensive and shallow groundwater connectivity in a cold desert ecosystem. Bull. Geol. Soc. Am. 123, 2295–2311. https://doi.org/10.1130/B30436.1.

Levy, J.S., Fountain, A.G., Gooseff, M.N., Barrett, J.E., Vantreese, R., Welch, K.A., Berry Lyons, W., Nielsen, U.N., Wall, D.H., 2014. Water track modification of soil ecosystems in the Lake Hoare basin, Taylor Valley, Antarctica. Antarct. Sci. 26, 153–162. https://doi.org/10.1017/S095410201300045X.

Lyons, W.B., Welch, K.A., Carey, A.E., Doran, P.T., Wall, D.H., Virginia, R.A., Fountain, A.G., Csath, B.M., Tremper, C.M., 2005. Groundwater seeps in Taylor Valley Antarctica: an example of a subsurface melt event. Ann. Glaciol. 40, 200–206. https://doi.org/10.3189/172756405781813609.

McKnight, D.M., Alger, A., Tate, C., Shupe, G., Spaulding, S., 1998. Longitudinal patterns in algal abundance and species distribution in meltwater streams in Taylor Valley, southern victoria land, Antarctica. In: Ecosystem Dynamics in a Polar Desert: the McMurdo Dry Valleys, Antarctica. American Geophysical Union, pp. 109–127. https://doi.org/10.1029/AR072p0109.

Myers, M.E., Doran, P.T., Myers, K.F., 2022. Valley-floor snowfall in Taylor Valley, Antarctica, from 1995 to 2017: spring, summer and autumn. Antarct. Sci. 34, 325–335. https://doi.org/10.1017/S0954102022000256.

Nielsen, U.N., Wall, D.H., Adams, B.J., Virginia, R.A., Ball, B.A., Gooseff, M.N., McKnight, D.M., 2012. The ecology of pulse events: insights from an extreme climatic event in a polar desert ecosystem. Ecosphere 3. https://doi.org/10.1890/ES11-00325.1 art17.

Obryk, M.K., Doran, P.T., Fountain, A.G., Myers, M., McKay, C.P., 2020. Climate from the McMurdo dry valleys, Antarctica, 1986–2017: surface Air temperature trends and redefined summer season. J. Geophys. Res. Atmos. 125, e2019JD032180 https://doi.org/10.1029/2019JD032180.

Olsen, S.R., Sommers, L.E., 1982. Phosphorus. In A.L. Page (ed.) Methods of soil analysis. Chemical and microbiological properties. Agronomy. Am. Soc. of Agron. 9 (2), 403–430. Madison, WI.

Pannewitz, S., Green, T.G.A., Scheidegger, C., Schlensog, M., Schroeter, B., 2003. Activity pattern of the moss Hennediella heimii (hedw.) zand. In the dry valleys, southern victoria land, Antarctica during the mid-austral summer. Polar Biol. 26, 545–551. https://doi.org/10.1007/s00300-003-0518-8.

Peddle, D.R., Hall, F.G., Ledrew, E.F., 1999. Spectral mixture analysis and geometric-optical reflectance modeling of boreal forest biophysical structure. Remote Sens. Environ. 67, 288–297. https://doi.org/10.1016/S0034-4257(98)00090-X.

Poage, M.A., Barrett, J.E., Virginia, R.A., Wall, D.H., 2008. The influence of soil geochemistry on nematode distribution, Mcmurdo Dry Valleys, Antarctica. Arctic Antarct. Alpine Res. 40, 119–128. https://doi.org/10.1657/1523-0430(06-051 [POAGE]2.0.CO;2.

Power, S.N., Salvatore, M.R., Sokol, E.R., Stanish, L.F., Barrett, J.E., 2020. Estimating microbial mat biomass in the McMurdo Dry Valleys, Antarctica using satellite imagery and ground surveys. Polar Biol. 43, 1753–1767. https://doi.org/10.1007/s00300-020-02742-y.

Power, S.N., Salvatore, M.R., Adams, B.J., Barrett, J.E., 2023. Hyperspectral Reflectance Values and Biophysicochemical Properties of Biocrusts and Soils in the Fryxell Basin, McMurdo Dry Valleys, Antarctica (2019). Environmental Data Initiative. https://doi.org/10.6073/pasta/a34f2a95ddae3f471fea0cab90a1e287.

Power, S.N., Thomas, V.A., Salvatore, M.R., Barrett, J.E., *In Preparation*. Habitat suitability of biocrust communities in a cold desert ecosystem.

Prokopy, W.R., 1995. In: Phosphorus in 0.5 M Sodium Bicarbonate Soil Extracts. QuikChem Method 12-115-01-1-B. Lachat Instruments, Milwaukee, WI.

R Core Team, 2017. R: A Language and Environment for Statistical Computing. R Foundation for Statistical Computing, Vienna, Austria. http://www.R-project.org.

Ramnarine, R., Voroney, R., Wagner-Riddle, C., Dunfield, K., 2011. Carbonate removal by acid fumigation for measuring the δ13C of soil organic carbon. Can. J. Soil Sci. 91, 247–250. https://doi.org/10.1139/CJSS10066.

Ramsey, M.S., Christensen, P.R., 1998. Mineral abundance determination: quantitative deconvolution of thermal emission spectra. J. Geophys. Res. 103, 577–596. https://doi.org/10.1029/97JB02784.

Roberts, D.A., Smith, M.O., Adams, J.B., 1993. Green vegetation, nonphotosynthetic vegetation, and soils in AVIRIS data. Remote Sens. Environ. 44, 255–269. https://doi.org/10.1016/0034-4257(93)90020-X.

Rodriguez-Caballero, E., Belnap, J., Büdel, B., Crutzen, P.J., Andreae, M.O., Pöschl, U., Weber, B., 2018. Dryland photoautotrophic soil surface communities endangered by global change. Nat. Geosci. 11, 185–189. https://doi.org/10.1038/s41561-018-0072-1.

Salvatore, M.R., 2015. High-resolution compositional remote sensing of the Transantarctic Mountains: application to the WorldView-2 dataset. Antarct. Sci. 27, 473–491. https://doi.org/10.1017/S095410201500019X.

Salvatore, M.R., Borges, S.R., Barrett, J.E., Sokol, E.R., Stanish, L.F., Power, S.N., Morin, P., 2020. Remote characterization of photosynthetic communities in the Fryxell basin of Taylor Valley, Antarctica. Antarct. Sci. 1–16 https://doi.org/10.1017/S0954102020000176.

Salvatore, M.R., Barrett, J.E., Borges, S.R., Power, S.N., Stanish, L.F., Sokol, E.R., Gooseff, M.N., 2021. Counting carbon: quantifying biomass in the McMurdo dry valleys through orbital & field observations. Int. J. Rem. Sens. 42, 8597–8623. https://doi.org/10.1080/01431161.2021.1981559.

Schimel, J.P., Bilbrough, C., Welker, J.M., 2004. Increased snow depth affects microbial activity and nitrogen mineralization in two Arctic tundra communities. Soil Biol. Biochem. 36, 217–227. https://doi.org/10.1016/j.soilbio.2003.09.008.

Schwarz, A.M.J., Green, T.G.A., Seppelt, R.D., 1992. Terrestrial vegetation at Canada glacier, southern victoria land, Antarctica. Polar Biol. 12, 397–404. https://doi.org/10.1007/BF00243110.

Simmons, B.L., Wall, D.H., Adams, B.J., Ayres, E., Barrett, J.E., Virginia, R.A., 2009a. Terrestrial mesofauna in above-and below-ground habitats: Taylor Valley, Antarctica. Polar Biol. 32, 1549–1558. https://doi.org/10.1007/s00300-009-0639-9.

Simmons, B.L., Wall, D.H., Adams, B.J., Ayres, E., Barrett, J.E., Virginia, R.A., 2009b. Long-term experimental warming reduces soil nematode populations in the McMurdo Dry Valleys, Antarctica. Soil Biol. Biochem. 41, 2052–2060. https://doi.org/10.1016/j.soilbio.2009.07.009.

Stanish, L.F., Nemergut, D.R., McKnight, D.M., 2011. Hydrologic processes influence diatom community composition in Dry Valley streams. J. North Am. Benthol. Soc. 30, 1057–1073. https://doi.org/10.1899/11-008.1.

Stanish, L.F., Kohler, T.J., Esposito, R.M.M., Simmons, B.L., Nielsen, U.N., Wall, D.H., Nemergut, D.R., McKnight, D.M., 2012. Extreme streams: flow intermittency as a control on diatom communities in meltwater streams in the McMurdo Dry Valleys, Antarctica. Can. J. Fish. Aquat. Sci. 69, 1405–1419. https://doi.org/10.1139/f2012-022.

Stone, M., Devlin, S., Hawes, I., Welch, K.A., Gooseff, M.N., Takacs-Vesbach, C.D., Morgan-Kiss, R.M., Adams, B.J., Barrett, J.E., Priscu, J.C., Doran, P.T., n.d.. *Accepted*. McMurdo Dry Valley Lake Edge "moats": the Ecological Intersection between Terrestrial and Aquatic Polar Desert Habitats. Antarct.Sci.

Thrane, J.-E., Kyle, M., Striebel, M., Haande, S., Grung, M., Rohrlack, T., Andersen, T., 2015. Spectrophotometric analysis of pigments: a critical assessment of a high-throughput method for analysis of algal pigment mixtures by spectral deconvolution. PLoS One 10, e0137645. https://doi.org/10.1371/journal.pone.0137645.

Treonis, A., Wall, D., Virginia, R., 1999. Invertebrate biodiversity in antarctic dry valley soils and sediments. Ecosystems 2, 482–492. https://doi.org/10.1007/s100219900096.

Trnková, K., Barták, M., 2017. Desiccation-induced changes in photochemical processes of photosynthesis and spectral reflectance in Nostoc commune (Cyanobacteria, Nostocales) colonies from polar regions. Phycol. Res. 65, 44–50. https://doi.org/10.1111/pre.12157.

Tucker, C.J., 1979. Red and photographic infrared linear combinations for monitoring vegetation. Remote Sens. Environ. 8, 127–150. https://doi.org/10.1016/0034-4257(79)90013-0.

Van Horn, D.J., Van Horn, M.L., Barrett, J.E., Gooseff, M.N., Altrichter, A.E., Geyer, K.M., Zeglin, L.H., Takacs-Vesbach, C.D., 2013. Factors controlling soil microbial biomass and bacterial diversity and community composition in a cold desert ecosystem: role of geographic scale. PLoS One 8, e66103. https://doi.org/10.1371/journal.pone.0066103.

Van Horn, D.J., Wolf, C.R., Colman, D.R., Jiang, X., Kohler, T.J., McKnight, D.M., Stanish, L.F., Yazzie, T., Takacs-Vesbach, C.D., 2016. Patterns of bacterial biodiversity in the glacial meltwater streams of the McMurdo Dry Valleys, Antarctica. FEMS Microbiol. Ecol. 92. https://doi.org/10.1093/femsec/fiw148.

Vignon, É., Roussel, M.-L., Gorodetskaya, I.V., Genthon, C., Berne, A., 2021. Present and future of rainfall in Antarctica. Geophys. Res. Lett. 48 https://doi.org/10.1029/2020gl092281.

Walthert, L., Graf, U., Kammer, A., Luster, J., Pezzotta, D., Zimmermann, S., Hagedorn, F., 2010. Determination of organic and inorganic carbon, δ 13 C, and nitrogen in soils containing carbonates after acid fumigation with HCl. J. Plant Nutr. Soil Sci. 173, 207–216. https://doi.org/10.1002/jpln.200900158.

Warren, S.G., 1982. Optical properties of snow. Rev. Geophys. Space Phys. 20, 67–89.

Weber, B., Belnap, J., Büdel, B., Antoninka, A.J., Barger, N.N., Chaudhary, V.B., Darrouzet-Nardi, A., Eldridge, D.J., Faist, A.M., Ferrenberg, S., Havrilla, C.A., Huber-Sannwald, E., Malam Issa, O., Maestre, F.T., Reed, S.C., Rodriguez-Caballero, E., Tucker, C., Young, K.E., Zhang, Y., Zhao, Y., Zhou, X., Bowker, M.A., 2022. What is a biocrust? A refined, contemporary definition for a broadening research community. Biol. Rev. Camb. Phil. Soc. 97, 1768–1785. https://doi.org/10.1111/brv.12862.

Wlostowski, A.N., Gooseff, M.N., McKnight, D.M., Jaros, C., Lyons, W.B., 2016. Patterns of hydrologic connectivity in the McMurdo Dry Valleys, Antarctica: a synthesis of 20 years of hydrologic data. Hydrol. Process. 30, 2958–2975. https://doi.org/10.1002/hyp.10818.

Wlostowski, A.N., Schulte, N.O., Adams, B.J., Ball, B.A., Esposito, R.M.M., Gooseff, M.N., Lyons, W.B., Nielsen, U.N., Virginia, R.A., Wall, D.H., Welch, K.A., McKnight, D.M., 2019. The hydroecology of an ephemeral wetland in the McMurdo dry valleys, Antarctica. J. Geophys. Res. Biogeosci. 124, 3814–3830. https://doi.org/10.1029/2019jg005153.

Xue, X., Adhikari, B.N., Ball, B.A., Barrett, J.E., Miao, J., Perkes, A., Martin, M., Simmons, B.L., Wall, D.H., Adams, B.J., 2023. Ecological stoichiometry drives the evolution of soil nematode life history traits. Soil Biol. Biochem. 177, 108891 https://doi.org/10.1016/j.soilbio.2022.108891.

Young, K.E., Reed, S.C., 2017. Spectrally monitoring the response of the biocrust moss Syntrichia caninervis to altered precipitation regimes. Sci. Rep. 7, 1–10. https://doi.org/10.1038/srep41793.